

# AutoDIR: Automatic All-in-One Image Restoration with Latent Diffusion

Yitong Jiang\* Zhaoyang Zhang\* Tianfan Xue Jinwei Gu  
The Chinese University of Hong Kong

{ytjiang@link, zhaoyangzhang@link, tfxue@ie, jwgu@cse}.cuhk.edu.hk

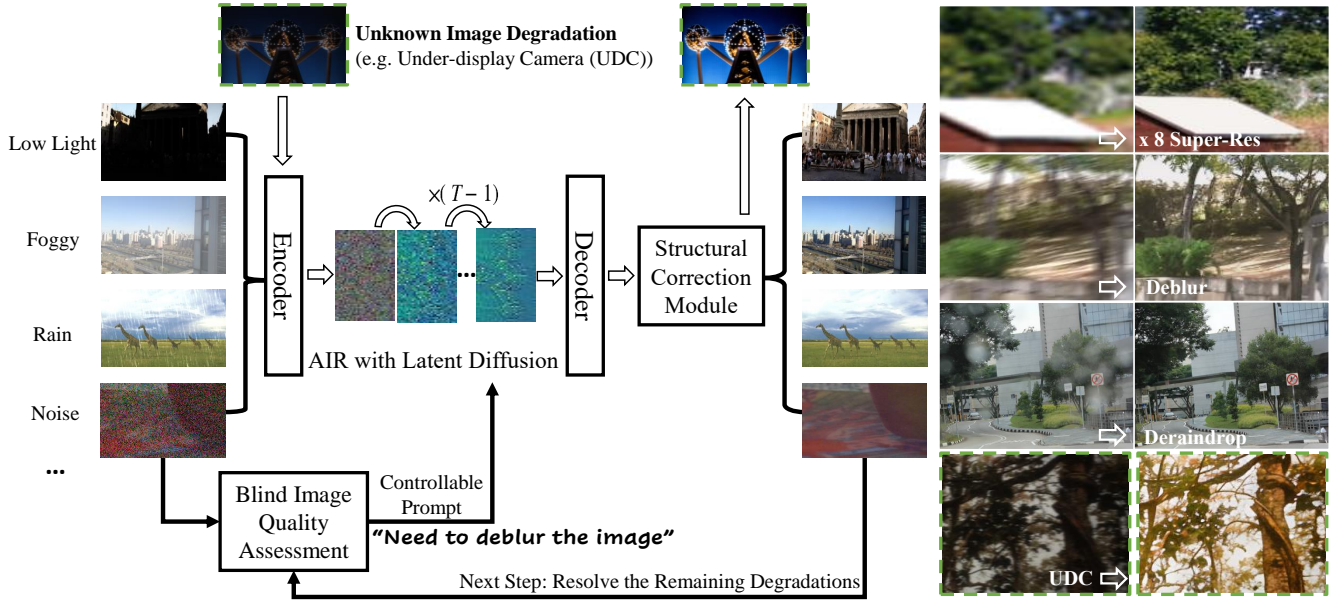


Figure 1. We propose AutoDIR, an automatic all-in-one model for image restoration capable of handling multiple types of image degradations, including low light, foggy, etc. **Left**: the pipeline for multi-task image restoration via AutoDIR, where the Blind Image Quality Assessment (BIQA) module detects the dominant degradations of the corrupted image and instructs the latent-diffusion-based All-in-One Image Restoration module (AIR) with a text prompt for restoration. The Structural Correction module (SCM) further improves the details of the restored images. For images with unknown degradations, e.g. the Under-display Camera image bordered by green dashed lines, AutoDIR automatically decomposes the task into multiple steps. **Right**: AutoDIR effectively restores clean images from different degradations and can handle images with unknown degradations. (**Zoom in for details**)

## Abstract

We propose an all-in-one image restoration system with latent diffusion, named AutoDIR, which can automatically detect and restore images with multiple unknown degradations. Our main hypothesis is that many image restoration tasks, such as super-resolution, motion deblur, denoising, low-light enhancement, dehazing, and deraining can often be decomposed into some common basis operators which improve image quality in different directions. AutoDIR aims to learn one unified image restoration model capable of performing these basis operators by joint training with multiple image restoration tasks. Specifically, AutoDIR consists of a

Blind Image Quality Assessment (BIQA) module based on CLIP which automatically detects unknown image degradations for input images, an All-in-One Image Restoration (AIR) module based on latent diffusion which handles multiple types of image degradation, and a Structural-Correction Module (SCM) which further recovers the image structures. Extensive experimental evaluation demonstrates that AutoDIR outperforms state-of-the-art approaches for a wider range of image restoration tasks. The design of AutoDIR also enables flexible user control (via text prompt) and generalization to new tasks as a foundation model of image restoration.

\*Equal contribution

## 1. Introduction

Restoring scene details and improving image quality is often the very first step of any computer vision system, which significantly determines the overall system performance. Depending on the operating environments and the signal processing pipelines, images captured by real-world computer vision systems often undergo multiple unknown degradations, such as noise, resolution loss, motion blur, defocus, color imbalance, chromatic aberration, haze, flare, distortion, etc. Previous image restoration methods often address these image degradations separately, including deblurring [23, 68], denoising [45, 78] deraining [24, 48], super-resolution [9, 62], low-light enhancement [37, 76], deraindrop [43], and dehaze [44, 55], by using specific single-task models. While these single-task approaches yield promising results within their respective tasks, they encounter difficulties when applied to complex real-world situations that involve multiple unknown degradations or require multiple steps of enhancement.

Is it possible to learn a unified “foundation” model for image restoration with the capability for automatically handling real-world images with multiple unknown degradations? The intuition is straightforward. Many individual image restoration tasks can often be grouped together as they aim to improve image quality along several major dimensions. For example, super-resolution and deblurring are similar because both aim to recover scene details, both denoising and deraining aim to remove image artifacts, and both dehazing and low-light enhancement aim to adjust the overall image tone and color. Therefore, there may exist a latent space for image restoration constructed along these dimensions, where some common basis image restoration operators can be composed together to restore corrupted images with multiple unknown degradations.

To this end, we propose an all-in-one image restoration system with latent diffusion, named AutoDIR, which can automatically detect and restore images with unknown degradations. Specifically, as shown in Figure 1, AutoDIR consists of three parts. The Blind Image Quality Assessment (BIQA) module, fine-tuned from a pre-trained language-vision model CLIP [46], is used to detect dominant image degradation types and generate corresponding text prompts. The All-in-One Image Restoration (AIR) module, fine-tuned from a pre-trained latent diffusion model [49], is used to perform the basic image restoration operators with the guidance of the text prompts from BIQA. Finally, the Structural Correction module (SCM) is a lightweight convolution network which further recovers image structures and corrects remaining image distortions. AutoDIR also enables flexible user control and editing at run-time, simply by alternating the text prompts generated by BIQA or providing additional text prompts.

To evaluate the effectiveness and generalization abil-

ity of AutoDIR, we have conducted a comprehensive set of experiments encompassing seven image restoration tasks, including denoising, motion deblurring, low-light enhancement, dehazing, deraining, deraindrop, and super-resolution. Experimental results show that AutoDIR outperforms consistently state-of-the-art methods. AutoDIR is also evaluated for the restoration of images captured by under-display cameras as well as underwater cameras, which are examples of imaging systems with multiple unknown degradations. Please refer to Sec. 4 for details.

## 2. Related Work

**Unified All-in-One Image Restoration** Previous approaches for unified all-in-one image restoration can be categorized into two main groups: unsupervised generative prior-based methods [3, 5, 15, 21, 25, 36, 40, 66, 70] and end-to-end supervised learning-based methods [12, 29, 31, 41, 58, 74]. Generative priors for image restoration have been widely exploited for image restoration, in the form of generative adversarial networks (GANs) inversion and filters [3, 5, 17, 21, 36, 40], VQ cookbooks [8, 33, 59, 79], latent diffusion models [15, 25, 66]. End-to-end supervised learning-based methods typically learn image embeddings extracted by an auxiliary degradation predictor to guide the image restoration model [29, 31, 41, 58, 74]. For example, Valanarasu et al. [58] leverage a transformer encoder to capture hierarchical features of haze, while Li et al. [30] employ a degradation classifier trained using contrastive learning. Park et al. [41] design a degradation classifier for multiple types of degradation to select appropriate Adaptive Discriminant filters, altering network parameters based on specific degradations. Nevertheless, these methods often rely on specific image degradation functions, which constrain the types of degradations they can handle. In contrast, with a BIQA (Blind Image Quality Assessment) module, the proposed AutoDIR is able to unify complex degradations without relying on assumptions about the specific degradation functions.

**Text-based Image Synthesis and Editing** Early works [56, 69, 72, 73, 82] on text-to-image synthesis and editing primarily relied on generative adversarial networks (GANs) [16]. Recently, developments in diffusion models [20, 49] and language-vision models [46] have led to significant progress in text-based image synthesis and editing [7, 39, 47, 51]. The emergence of diffusion-based methods has offered new avenues for text-to-image editing, which can be broadly categorized into data-driven [4] and no-extra-data-required approaches [18, 26, 77]. In the data-driven category, Brooks et al. [4] employ a stable diffusion model fine-tuned with a large dataset of text prompt and image pairs. However, it is primarily designed for semantic image editing and struggles to deliver satisfactory results in

tasks related to image quality enhancement. On the other hand, some methods focus on image editing without extra training data. For instance, recent works interpolate the text embedding [26] or score estimate [77] of the input and desired images. However, it requires individual finetuning of the diffusion model for each input image, leading to time-consuming operations. Hertz et al. [18] improve editing efficiency by directly manipulating cross-attention maps without the need for per-image finetuning. However, it requires interior maps in the reversing process and is thus not applicable to real image editing. Unlike the above methods, AutoDIR supports real image enhancement without per-image finetuning.

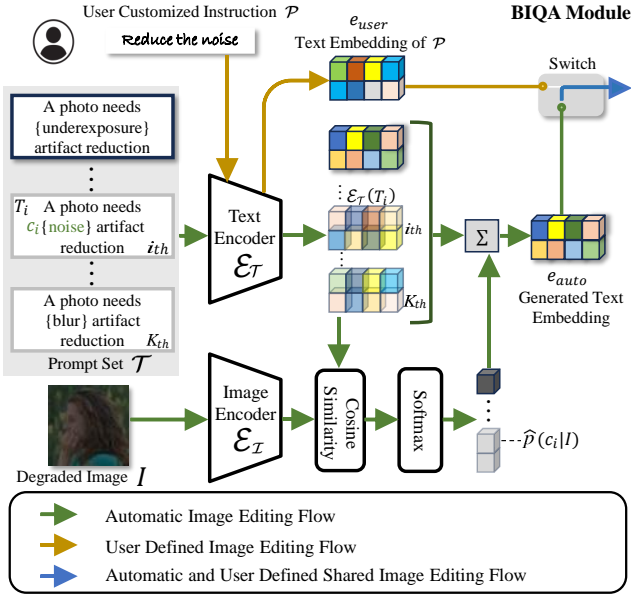


Figure 2. Diagram of the proposed Blind Image Quality Assessment (BIQA) module. Refer to Section 3.1 for more details.

### 3. Our Method

Figure 1 shows the overall flowchart of the proposed AutoDIR (Automatic All-in-One Image Restoration with Latent Diffusion), a unified model that can automatically detect and address multiple unknown degradations in images. AutoDIR consists of three parts:

- **Blind Image Quality Assessment (BIQA):** This module automatically identifies the predominant degradations present in the input image, such as noise, blur, haze, and generates a corresponding text prompt, denoted as  $e_{auto}$ , which is subsequently used in the image restoration process.
- **All-in-one Image Restoration (AIR):** This module is finetuned based on a pre-trained latent diffusion model [49]. With the guidance from the text embedding  $e_{auto}$  from BIQA (or user-provided), the AIR module outputs a re-

stored image  $I_{sd}$ .

- **Structural-correction module (SCM):** SCM is a lightweight convolution network that aims to further restore image details and correct remaining distortions in  $I_{sd}$ . The output of this restoration process is the final restored image, denoted as  $I_{res}$ .

#### 3.1. Blind Image Quality Assessment (BIQA)

We utilize a CLIP model [46] as our BIQA backbone. However, since CLIP is pre-trained for visual recognition tasks emphasizing semantic information rather than image quality, it cannot be directly used for BIQA. To overcome this, we tackle the problem in two steps: (i) We construct a new image quality assessment task for fine-tuning CLIP. (ii) We propose a new regularization term for image-quality-aware training.

As illustrated in Fig. 2, let  $\mathcal{C}$  denotes the set of image distortions, i.e.  $\mathcal{C} = \{c_1, c_2, \dots, c_K\}$ , where  $c_i$  is an image distortion type, e.g. “noise” and  $K$  is the number of distortions we consider. The textural description prompt set is  $\mathcal{T} = \{T | T = \text{“A photo needs } \{c_i\} \text{ artifact reduction.”}, c \in \mathcal{C}\}$ . Given a corrupted image  $I$  which undergoes several unknown artifacts, our BIQA aims to identify the dominant degradation of  $I$  and extract the corresponding text embedding. BIQA consists of an image encoder  $\mathcal{E}_I$  and a text encoder  $\mathcal{E}_T$ . We first obtain the image embedding  $\mathcal{E}_I(I) \in \mathbb{R}^d$  and the text embedding  $\mathcal{E}_T(T) \in \mathbb{R}^{K \times d}$ , then we compute the cosine similarity between image embedding  $\mathcal{E}_I(I)$  and each prompt embedding  $\mathcal{E}_T(T_i) \in \mathbb{R}^d$  by:

$$\text{logit}(c_i|I) = \frac{\mathcal{E}_I(I) \cdot \mathcal{E}_T(T_i)}{\|\mathcal{E}_I(I)\|_2 \|\mathcal{E}_T(T_i)\|_2}, \quad (1)$$

where  $T_i$  is the  $i$ -th element of  $\mathcal{T}$ . Next, we calculate the probability  $\hat{p}(c_i|I)$  and obtain the output text embedding of BIQA  $e_{auto}$  by:

$$\hat{p}(c_i|I) = \frac{\exp(\text{logit}(c_i|I))}{\sum_{i=1}^K \exp(\text{logit}(c_i|I))}, \quad (2)$$

$$e_{auto} = \sum_{i=1}^K \hat{p}(c_i|I) \mathcal{E}_T(T_i). \quad (3)$$

During the optimization of BIQA, we freeze the parameters of the text encoder  $\mathcal{E}_T$  and finetune the image encoder  $\mathcal{E}_I$  using the multi-class fidelity loss [57]. The fidelity loss can be denoted as:

$$L_{FID} = 1 - \sum_{i=1}^K \sqrt{y(c_i|I) \hat{p}(c_i|I)}, \quad (4)$$

where  $y(c_i|I)$  is a binary variable that equals 1 if  $c_i$  is the dominant degradation in image  $I$ , and 0 otherwise.



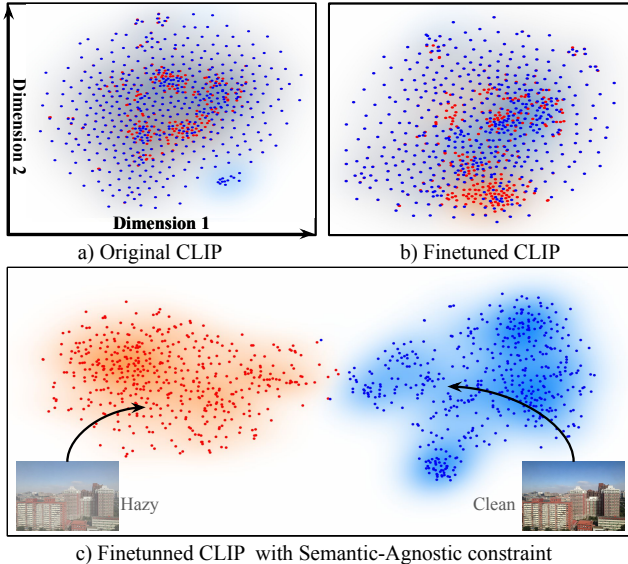


Figure 3. t-SNE visualization of image embeddings  $\mathcal{E}_{\mathcal{I}}(I)$  of CLIP of Blind Image Quality Assessment (BIQA) on SOTs dehazing dataset [28]. Image embeddings of foggy images and their ground-truth clean images are extracted by a) original CLIP. b) finetuned CLIP. c) CLIP finetuned with semantic-agnostic constraint. This illustrates that semantic-agnostic constraint can separate the embeddings of the degraded images from the clean images, while original CLIP and finetuned CLIP features cannot.

In addition to the automatic text embedding generated by the BIQA module ( $e_{auto}$ ), AutoDIR also supports user-defined prompts for customized control. Given a user instruction  $\mathcal{P}$ , we can also extract the text embedding  $e_{user} = \mathcal{E}_{\mathcal{T}}(\mathcal{P})$  as additional guidance for image restoration.

**Semantic-Agnostic Constraint for Blind Image Quality Assessment.** Since the original CLIP model is pre-trained on tasks such as image classification, its corresponding  $\mathcal{E}_{\mathcal{I}}(I)$  encoders tend to encode images based on their semantic information (e.g., cat or dog) rather than their image quality (e.g., noisy or clean). When we fine-tune the CLIP model for generating texts for BIQA according to image quality, this becomes a significant limitation. As shown in Fig. 3 a) and b), the image embeddings extracted by the original CLIP and the finetuned CLIP on foggy, as well as their corresponding ground-truth clean images, cannot be separated, indicating a focus on semantic information rather than image quality differences.

To address this issue, we propose a novel approach called the semantic-agnostic constraint loss ( $L_{SA}$ ) to regulate the fine-tuning process and prevent the model from relying solely on semantic information rather than image quality. The semantic-agnostic loss ( $L_{SA}$ ) applies a penalty when the CLIP model suggests that the artifact  $c_i$  is present in the ground-truth clean image  $I_{gt}$  which corresponds to the

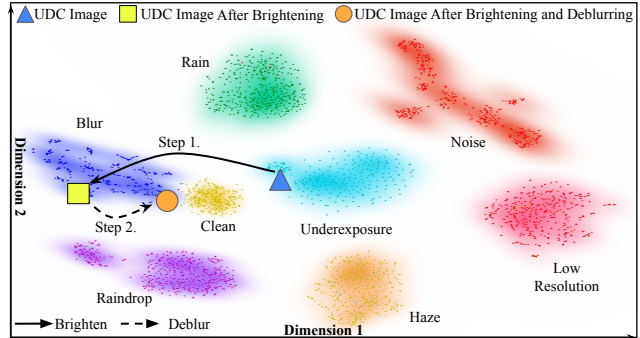


Figure 4. t-SNE visualization of image embeddings  $\mathcal{E}_{\mathcal{I}}(I)$  with seven types of degradations, which illustrates the space of common image degradations. Images captured by Under-Display Cameras (UDC) [81] suffer from both blur and underexposure. AutoDIR automatically decides (via BIQA) the first step is to improve "underexposure", and the second step is to remove "blur", moving the input images towards the region of clean images.

degraded image  $I$ . This penalty forces the BIQA model to distinguish between  $I_{gt}$  and  $I$  based on image quality, encouraging the CLIP image encoder ( $\mathcal{E}_{\mathcal{I}}(I)$ ) to focus on extracting image quality information rather than semantic information. This constraint loss can be derived using the following equation:

$$L_{SA} = \sum_{i=1}^K \sqrt{y(c_i|I)\hat{p}(c_i|I_{gt})}, \quad (5)$$

where  $y(c_i|I)$  is a binary variable that is equal to 1 if  $c_i$  represents the dominant degradation in image  $I$ , and 0 otherwise, and  $\hat{p}(c_i|I_{gt})$  denotes the probability that the dominant degradation in  $I_{gt}$  is represented by  $c_i$ .

We incorporate the semantic-agnostic constraint  $L_{SA}$  with the fidelity loss  $L_{FID}$ , resulting in the total loss  $L_{BIQA}$  for BIQA module:

$$L_{BIQA} = L_{FID} + \lambda L_{SA}, \quad (6)$$

where we set  $\lambda = 1$  in our experiments. As shown in Fig. 3 c), CLIP fine-tuned with a semantic-agnostic constraint can separate the embeddings of the degraded images from the clean images as expected.

### 3.2. All-in-one Image Restoration (AIR)

The second part of AutoDIR is the All-in-one Image Restoration (AIR) module, which is designed to apply various image restoration operators. Fig. 4 shows the t-SNE visualization of image embeddings  $\mathcal{E}_{\mathcal{I}}(I)$  with seven types of degradations, which illustrates the space of common image degradations. AutoDIR is able to handle images with unknown degradations. For example, the images captured by Under-Display Cameras (UDC) [81] suffer from both blur



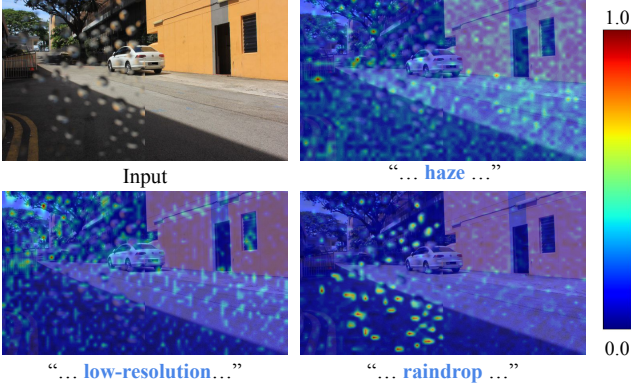


Figure 5. Cross-attention maps of text-conditioned diffusion image restoration. The top-left shows an input image with raindrops on the left half. The remaining plots show the cross-attention masks for the keywords “haze”, “low-resolution” and “raindrop” in the text prompt used for restoration. While the cross-attention maps for “haze” and “low-resolution” are more uniformly distributed over the entire image, the map for “raindrop” correctly focuses on the actual image artifacts, as expected.

and underexposure. AutoDIR automatically decides (via BIQA) the first operator is to improve “underexposure”, and the second operator is to remove “blur”, moving the input images towards the region of clean images.

The AIR module is designed based on the Latent Diffusion Model [49], utilizing both text and image embedding conditions to restore images  $I_{sd}$  with generative priors. The text embedding condition, denoted as  $e = \{e_{auto}, e_{user}\}$ , aims to disentangle different types of image degradations, while the latent image embedding condition  $z_I = \mathcal{E}_{ldm}(I)$  from the image encoder  $\mathcal{E}_{ldm}$  of the latent diffusion model [49] is to provide information of image structures. To enable the text condition to guide different image restoration, we incorporate cross-attention [60] to map the text condition  $e$  into the intermediate layers of the time-conditional UNet backbone [50] of the Latent Diffusion Model [49]. For the image condition, we concatenate the image condition  $z_I$  with the noisy latent  $z_t$  and feed them to the UNet backbone. Consequently, the denoiser expression of the UNet backbone becomes  $\epsilon_\theta(e, [z_t, z_I], t)$ , where  $[\cdot]$  denotes concatenation. After the reversing process, we obtain the restored image  $I_{sd}$  by passing the updated latent  $\hat{z}$  through the decoder  $\mathcal{D}$  of the Latent Diffusion Model, defined as  $I_{sd} = \mathcal{D}(\hat{z})$ . During training, we fine-tune the UNet backbone  $\epsilon_\theta(e, [z_t, z_I], t)$  for image restoration tasks. The objective function is defined as:

$$L_{AIR} = \mathbb{E}_{\mathcal{E}_{ldm}(x), c_I, e, \epsilon, t} [\|\epsilon - \epsilon_\theta(e, [z_t, z_I], t)\|_2^2]. \quad (7)$$

Fig. 5 shows our experiment of exploring the mechanism of the text conditions disentangling different image restoration tasks during the reverse diffusion process. We find that different text conditions yield different cross-attention



Figure 6. The Structural-Correction Module (SCM) is an additional convolution network to further improve image structures and details. As shown, image structures, i.e., human face and text, are severely distorted without SCM and recovered well with SCM.

maps. As shown in Fig. 5, changing the text prompt leads to significant changes in the cross-attention map. The map closely aligns with the text prompt, which either uniformly distributes attention across the entire image for the “dehazing” prompt, or concentrates on the part with edges or textures for the “low-resolution” prompt, or focuses on specific areas such as raindrops for the “deraindrop” prompt. This shows that BIQA and AIR can guide the diffusion attention toward regions that are more likely to have image artifacts.

### 3.3. Structural-Correction Module (SCM)

While the latent-diffusion-based generative modes can hallucinate texture details, they sometimes struggle to maintain fine image structures such as human faces and texts as shown in Fig. 6. To address the structure distortion caused by the AIR module, we employ an efficient structural-correction module (SCM) denoted as  $\mathcal{F}$ . The purpose of SCM is to extract the contextual information  $\mathcal{R}$  from the original image and incorporate it with the intermediate image restoration result  $I_{sd}$  in a residual manner. This is achieved through the following equation:

$$I_{res} = I_{sd} + w \cdot \mathcal{F}([I_{sd}, I]), \quad (8)$$

where  $[\cdot]$  denotes concatenation, and  $w$  is an adjustable coefficient that ranges between 0 and 1. The value of  $w$  determines the extent to which contextual information is utilized to recover the final result. A larger value of  $w$  emphasizes the use of contextual information, which is beneficial for tasks that require structure consistency, such as low light enhancement. Conversely, a smaller value of  $w$  is often employed to maintain the generation capability of AIR for tasks like super-resolution. By integrating SCM, AutoDIR effectively restores the distorted context of the original image, seamlessly incorporating the enhancements made during the editing phase as shown in Fig. 6.

When training SCM, instead of sampling the edited latent  $\hat{z}_t$ , which is time-consuming, we utilize the estimated edited latent  $\tilde{z}$ , which is calculated by:

$$\tilde{z} = \frac{z_t}{\sqrt{\alpha}} - \frac{\sqrt{1 - \alpha}\epsilon_\theta(e, [z_t, z_I], t)}{\sqrt{\alpha}}, \quad (9)$$

where  $\bar{\alpha}$  represents the noise scheduler introduced in [49]. The loss function for SCM is further defined as:

$$L_{SCM} = \|I_{gt} - (\mathcal{F}(\mathcal{D}(\tilde{z}), I) + \mathcal{D}(\tilde{z}))\|_2^2 \quad (10)$$

## 4. Experiments

We evaluated AutoDIR on seven representative image restoration tasks as well as two tasks with unknown image degradations. To fully validate the feasibility and effectiveness of unifying multiple restoration and enhancement tasks, we compare AutoDIR with both CNN-based [10] and Diffusion-based multitasking [49] backbones. Please refer to the appendix for implementation details. The source code and trained models will be released upon publication.

**Datasets** The seven image restoration tasks are denoising, deblurring, super-resolution, low-light enhancement, dehazing, deraining, and deraindrop. For denoising, we use SIDD [1] and a synthetic noise dataset with DIV2K [2] and Flickr2K [32]. For super-resolution, we follow previous practice and train AutoDIR with DIV2K [2] and Flickr2K [32] training sets, with jointly downsampled images at x8 and x4 scales as inputs. In addition, we use GoPro [38], LOL [67], RESIDE [28], Rain200L [71], and Raindrop [42] for deblurring, low-light enhancement, dehazing, deraining, and deraindrop, respectively. During inference, we evaluate multiple test sets. These include SIDD [1], CBSD68 [35], DIV2K [2], GoPro [38], HIDE [53], LOL [67], SOTS-Outdoor [28], Rain100 [71], and Raindrop [42], each corresponding to their respective tasks. For experiments with unknown degradations, we use the Under-Display Camera (TOLED) dataset [81], the Enhancing Underwater Visual Perception (EUVP) dataset [22], and the Snow Dataset (CSD) dataset [11].

**Evaluation Metrics** Many widely used metrics for image quality assessment, such as PSNR and SSIM, do not always correlate well with human visual perception. In our study, we employ a recently developed metric DISTS [13] which is shown to align well with human perception and optimal for image restoration [14]. In addition, for completeness, we also report PSNR and LPIPS [75]. For the super-resolution and deblurring task, we adopt the widely used blind perceptual metrics including CLIP-IQA [61] and MUSIQ [27] to evaluate the quality of generated images following [6, 62, 65].

### 4.1. Results on Multi-task Image Restoration

We first evaluate AutoDIR across seven image restoration tasks. We compare with two state-of-the-art methods: the CNN-based single-task image restoration pipeline NAFNet [10] and the generative backbone Stable Diffusion [49]. Both NAFNet and Stable Diffusion are fine-tuned for all seven tasks, employing an identical training configuration to AutoDIR.

Table 1 and Table 2 present quantitative results of AutoDIR and other methods in all seven tasks. As demonstrated, AutoDIR achieves competitive performance across all seven tasks and significantly outperforms both NAFNet [10] and Stable Diffusion [49], as indicated by a substantial margin in the average score. We also show the qualitative comparison results on the seven image restoration tasks in Fig. 7 and Fig. 8, which demonstrate that AutoDIR can achieve more visually appealing results than the other baselines. A comprehensive and detailed analysis of the quantitative and qualitative results for each specific task can be found in the appendix.

### 4.2. Results on Multiple Unknown Degradations

To show that AutoDIR is able to handle multiple unknown image degradations, we conducted experiments on two additional datasets: the Under-Display-Camera (TOLED) dataset [80] and the Enhancing Underwater Visual Perception (EUVP) dataset [22]. These two datasets consist of multiple unknown image degradations and are completely excluded for training, allowing us to evaluate the performance of AutoDIR in handling unknown, diverse image distortions. Fig. 9 demonstrates the iterative process of AutoDIR to handle images from these two datasets. As shown, AutoDIR is able to automatically decompose the UDC restoration in two steps (“brightening” and “deblurring”) and the Underwater restoration in two steps (“deblurring” and “dehazing”) and restore the input images. For comparison, we also show the results of a recent diffusion-based zero-shot image restoration method GDP [15].

### 4.3. Ablation Studies

The first ablation study is to validate the importance of the BIQA and SCM modules, as shown in Table 3. The presence of proper guidance from the BIQA module is crucial for enabling accurate image restoration or enhancement in complex tasks. As shown in Table 3, incorporating the BIQA model into the AutoDIR pipeline consistently improves performance in multitasking scenarios. Similarly, the SCM module is designed to maintain fine image structures after the latent-diffusion-based image restoration. Table 3 also showed that incorporating the SCM module consistently achieves performance gains.

Our second ablation study is to investigate the possibility of using the all-in-one image restoration (AIR) module as a foundation model for general image restoration, which is based on the hypothesis that joint learning of multiple image restoration tasks may result in basis operators that are useful for other image restoration tasks. Inspired by prior work on vision foundation models [54, 64, 83], we conduct experiments on the unseen de-snowing task to evaluate this hypothesis. For our experiments, we utilize 90 snowy-clean image pairs of the Comprehensive Snow





Figure 7. Qualitative comparisons with NAFNet [10] and Stable Diffusion (SD) [49] on denoising,  $\times 8$  super-resolution, and deblurring tasks. See the Appendix for more results (**Zoom in for better view**).

Table 1. Quantitative comparison on denoising, deraining, dehazing, deraindrop, and low light enhancement tasks. The best results are marked in boldface and the second-best results are underlined.

Method	Denoise						Derain			Dehaze			Deraindrop			Low light		
	Real			Synthetic			DISTS↓	PSNR↑	LPIPS↓	DISTS↓	PSNR↑	LPIPS↓	DISTS↓	PSNR↑	LPIPS↓	DISTS↓	PSNR↑	LPIPS↓
NAFNet	0.198	<b>37.08</b>	0.165	0.213	<u>27.64</u>	0.200	<u>0.093</u>	<u>30.46</u>	<u>0.100</u>	<u>0.055</u>	<u>26.75</u>	<u>0.038</u>	0.125	<u>25.04</u>	0.138	0.173	<b>21.15</b>	0.240
Stable Diffusion	<u>0.169</u>	32.64	<b>0.126</b>	<u>0.155</u>	22.58	<u>0.186</u>	0.114	23.21	0.147	0.071	23.49	0.091	<u>0.086</u>	24.84	<u>0.104</u>	<u>0.140</u>	18.97	<u>0.159</u>
<b>Ours</b>	<b>0.167</b>	<u>36.91</u>	<u>0.145</u>	<b>0.154</b>	<b>28.42</b>	<b>0.145</b>	<b>0.059</b>	<b>33.05</b>	<b>0.036</b>	<b>0.032</b>	<b>28.14</b>	<b>0.021</b>	<b>0.065</b>	<b>29.89</b>	<b>0.058</b>	<b>0.139</b>	<u>20.81</u>	<b>0.141</b>

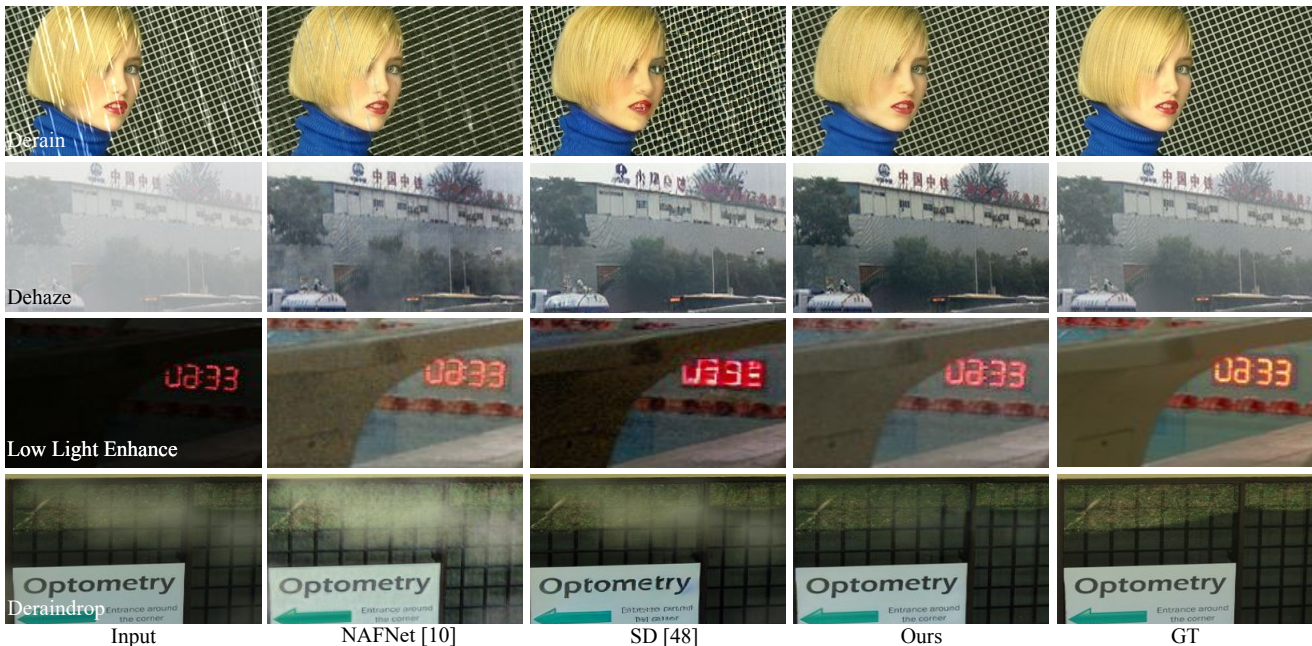


Figure 8. Qualitative comparisons with NAFNet [10] and Stable Diffusion (SD) [49] on deraining, dehazing, low light enhancement, and deraindrop tasks. See the Appendix for more results. (**Zoom in for better view**)

Dataset (CSD) [11] to fine-tune the AIR module which is initialized with the pre-trained AIR weights obtained from training on the seven tasks. Fig. 10 demonstrates the fine-tuned AIR module with the initialization of pre-trained

weight adapts to the de-snowing task more quickly compared to the module without the pre-trained weights. This shows the new image restoration task can benefit from the knowledge acquired from other image restoration tasks, in-





Figure 9. AutoDIR deals with multiple unknown image degradations. Iterative image restoration on unseen Under-Display Camera (TOLED) dataset [81] and unseen Enhancing Underwater Visual Perception (EUVP) dataset [22]. Left: input image. Second: step-one restored images and text prompts. Third: step-two restored images and text prompts. Last: zero-shot method GDP [15] for comparison.

Table 2. Quantitative comparison on deblurring and single image super-resolution x8 tasks. PSNR/MUSIQ/CLIP-IQA  $\uparrow$ : the higher, the better; DIST/LPIPS $\downarrow$ : the lower, the better.

Method	Deblur					Super Resolution				
	DISTS	MUSIQ	CLIP-IQA	PSNR	LPIPS	DISTS	MUSIQ	CLIP-IQA	PSNR	LPIPS
NAFNet	<u>0.149</u>	43.28	0.221	<u>26.67</u>	<u>0.208</u>	0.313	21.31	0.279	<b>24.52</b>	0.554
SD	0.157	<u>44.83</u>	<u>0.255</u>	22.53	0.241	<u>0.238</u>	<u>33.54</u>	<u>0.365</u>	23.48	<u>0.380</u>
Ours	<b>0.117</b>	<b>53.73</b>	<b>0.278</b>	<b>26.86</b>	<b>0.156</b>	<b>0.215</b>	<b>48.99</b>	<b>0.472</b>	<u>23.57</u>	<b>0.301</b>

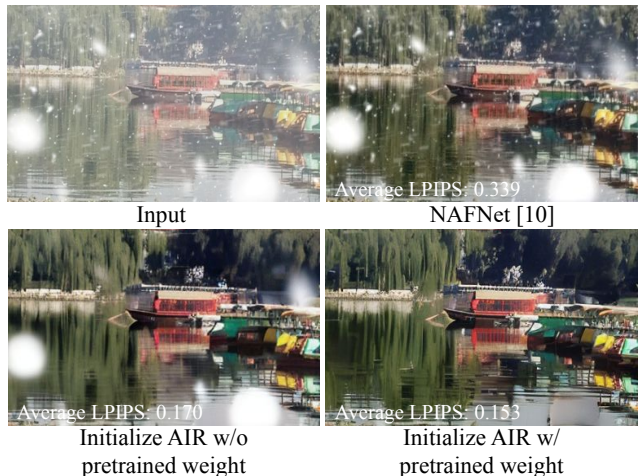


Figure 10. Qualitative comparisons on NAFNet [10], AIR module finetuned w/ and w/o weight pre-trained on seven tasks, along with quantitative evaluations based on the average LPIPS scores [75] achieved on unseen desnowing task.

Table 3. Ablation study on deraindrop and dehazing tasks.

Method	Deraindrop			Dehaze		
	DISTS $\downarrow$	PSNR $\uparrow$	LPIPS $\downarrow$	DISTS $\downarrow$	PSNR $\uparrow$	LPIPS $\downarrow$
w/o SCM & BIQA	0.086	24.84	0.104	0.071	23.49	0.091
w/o BIQA	0.075	28.84	0.068	0.038	27.62	0.025
w/o SCM	0.083	25.58	0.096	0.068	23.60	0.081
<b>AutoDIR</b>	<b>0.065</b>	<b>29.89</b>	<b>0.058</b>	<b>0.032</b>	<b>28.14</b>	<b>0.021</b>

dicating the implicit correlations between them. Moreover, it also outperforms the NAFNet specifically trained for the de-snowing task, which further shows the feasibility of constructing a foundational image restoration model by exploring the underlying correlations.

## 5. Conclusions and Discussions

In this paper, we present AutoDIR, an all-in-one image restoration system with latent diffusion, which is capable of restoring images with multiple unknown degradations. By jointly training from multiple individual image restoration datasets, AutoDIR can be viewed as a foundation model for image restoration, which can automatically detect and address multiple image degradations (with BIQA) and enables effective few-shot learning for novel tasks.

To our knowledge, AutoDIR is the most general comprehensive framework for automatic image restoration in the context of complex real-scenario images with multiple unknown degradations. We hope that this framework can provide a solid foundation for further works on complex real-scenario images and has the potential to be extended to various practical applications, such as local image enhancement and multi-task video restoration.

There are several limitations of AutoDIR that we plan to address in the future. First, the computational cost is similar to Stable Diffusion [49] and other diffusion-based image restoration methods [63], which is often significantly higher than non-generative networks such as NAFNet [10]. Some recent work on accelerating diffusion networks such as one-step diffusion [34] provides possible solutions. Second, AutoDIR currently focuses more on global image restoration, such as deblurring, denoising, and low-light enhancement, rather than local region-based image editing, such as flare removal and inpainting. Extending AutoDIR for local image editing by incorporating semantic segmentation may be an interesting direction to explore.

## References

- [1] Abdelrahman Abdelhamed, Stephen Lin, and Michael S. Brown. A high-quality denoising dataset for smartphone cameras. In *Proceedings of the IEEE Conference on Computer Vision and Pattern Recognition (CVPR)*, 2018. 6
- [2] Eirikur Agustsson and Radu Timofte. NTIRE 2017 challenge on single image super-resolution: Dataset and study. In *Proceedings of the IEEE Conference on Computer Vision and Pattern Recognition (CVPR) Workshops*, 2017. 6
- [3] David Bau, Hendrik Strobelt, William Peebles, Jonas Wulff, Bolei Zhou, Jun-Yan Zhu, and Antonio Torralba. Semantic photo manipulation with a generative image prior. *ACM Transactions on Graphics (TOG)*, 38(4):59, 2019. 2
- [4] Tim Brooks, Aleksander Holynski, and Alexei A Efros. InstructPix2Pix: Learning to follow image editing instructions. In *Proceedings of Advances in Neural Information Processing Systems (NeurIPS)*, 2023. 2
- [5] Kelvin CK Chan, Xintao Wang, Xiangyu Xu, Jinwei Gu, and Chen Change Loy. GLEAN: Generative latent bank for large-factor image super-resolution. In *Proceedings of the IEEE Conference on Computer Vision and Pattern Recognition (CVPR)*, 2021. 2
- [6] Kelvin CK Chan, Shangchen Zhou, Xiangyu Xu, and Chen Change Loy. Investigating tradeoffs in real-world video super-resolution. In *Proceedings of the IEEE Conference on Computer Vision and Pattern Recognition (CVPR)*, 2022. 6
- [7] Hila Chefer, Yuval Alaluf, Yael Vinker, Lior Wolf, and Daniel Cohen-Or. Attend-and-excite: Attention-based semantic guidance for text-to-image diffusion models. *ACM Transactions on Graphics (TOG)*, 42(4):1–10, 2023. 2
- [8] Chaofeng Chen, Xinyu Shi, Yipeng Qin, Xiaoming Li, Xiaoguang Han, Tao Yang, and Shihui Guo. Real-world blind super-resolution via feature matching with implicit high-resolution priors. 2022. 2
- [9] Chaofeng Chen, Xinyu Shi, Yipeng Qin, Xiaoming Li, Xiaoguang Han, Tao Yang, and Shihui Guo. Real-world blind super-resolution via feature matching with implicit high-resolution priors. In *IEEE Transactions on Multimedia (TMM)*, 2022. 2
- [10] Liangyu Chen, Xiaojie Chu, Xiangyu Zhang, and Jian Sun. Simple baselines for image restoration. In *Proceedings of European Conferences on Computer Vision (ECCV)*, 2022. 6, 7, 8, 1, 2, 3
- [11] Wei-Ting Chen, Hao-Yu Fang, Cheng-Lin Hsieh, Cheng-Che Tsai, I Chen, Jian-Jiun Ding, Sy-Yen Kuo, et al. All snow removed: Single image desnowing algorithm using hierarchical dual-tree complex wavelet representation and contradict channel loss. In *Proceedings of the IEEE International Conference on Computer Vision (ICCV)*, 2021. 6, 7
- [12] Wei-Ting Chen, Zhi-Kai Huang, Cheng-Che Tsai, Hao-Hsiang Yang, Jian-Jiun Ding, and Sy-Yen Kuo. Learning multiple adverse weather removal via two-stage knowledge learning and multi-contrastive regularization: Toward a unified model. In *Proceedings of the IEEE Conference on Computer Vision and Pattern Recognition (CVPR)*, 2022. 2
- [13] Keyan Ding, Kede Ma, Shiqi Wang, and Eero P. Simoncelli. Image quality assessment: Unifying structure and texture similarity. *IEEE Transactions on Pattern Analysis and Machine Intelligence (TPAMI)*, 2020. 6
- [14] Keyan Ding, Kede Ma, Shiqi Wang, and Eero Simoncelli. Comparison of full-reference image quality models for optimization of image processing systems. *International Journal of Computer Vision (IJCV)*, 129, 2021. 6
- [15] Ben Fei, Zhaoyang Lyu, Liang Pan, Junzhe Zhang, Weidong Yang, Tianyue Luo, Bo Zhang, and Bo Dai. Generative diffusion prior for unified image restoration and enhancement. In *Proceedings of the IEEE Conference on Computer Vision and Pattern Recognition (CVPR)*, 2023. 2, 6, 8
- [16] Ian Goodfellow, Jean Pouget-Abadie, Mehdi Mirza, Bing Xu, David Warde-Farley, Sherjil Ozair, Aaron Courville, and Yoshua Bengio. Generative adversarial nets. *Proceedings of Advances in Neural Information Processing Systems (NeurIPS)*, 2014. 2
- [17] Jinjin Gu, Yujun Shen, and Bolei Zhou. Image processing using multi-code GAN prior. In *Proceedings of the IEEE Conference on Computer Vision and Pattern Recognition (CVPR)*, 2020. 2
- [18] Amir Hertz, Ron Mokady, Jay Tenenbaum, Kfir Aberman, Yael Pritch, and Daniel Cohen-Or. Prompt-to-Prompt image editing with cross attention control. *Proceedings of International Conference on Learning Representations (ICLR)*, 2023. 2, 3
- [19] Jonathan Ho and Tim Salimans. Classifier-free diffusion guidance. In *Proceedings of Advances in Neural Information Processing Systems (NeurIPS) Workshops*, 2021. 1
- [20] Jonathan Ho, Ajay Jain, and Pieter Abbeel. Denoising diffusion probabilistic models. *Proceedings of Advances in Neural Information Processing Systems (NeurIPS)*, 2020. 2
- [21] Shady Abu Hussein, Tom Tirer, and Raja Giryes. Image-adaptive GAN based reconstruction. In *Proceedings of the AAAI Conference on Artificial Intelligence*, 2020. 2
- [22] Md Jahidul Islam, Youya Xia, and Junaed Sattar. Fast underwater image enhancement for improved visual perception. *IEEE Robotics and Automation Letters (RA-L)*, 2020. 6, 8, 3
- [23] Seo-Won Ji, Jeongmin Lee, Seung-Wook Kim, Jun-Pyo Hong, Seung-Jin Baek, Seung-Won Jung, and Sung-Jea Ko. XYDeblur: divide and conquer for single image deblurring. In *Proceedings of the IEEE Conference on Computer Vision and Pattern Recognition (CVPR)*, 2022. 2
- [24] Kui Jiang, Zhongyuan Wang, Peng Yi, Chen Chen, Baojin Huang, Yimin Luo, Jiayi Ma, and Junjun Jiang. Multi-scale progressive fusion network for single image deraining. In *Proceedings of the IEEE Conference on Computer Vision and Pattern Recognition (CVPR)*, 2020. 2
- [25] Bahjat Kawar, Michael Elad, Stefano Ermon, and Jiaming Song. Denoising diffusion restoration models. In *Proceedings of Advances in Neural Information Processing Systems (NeurIPS)*, 2022. 2
- [26] Bahjat Kawar, Shiran Zada, Oran Lang, Omer Tov, Huiwen Chang, Tali Dekel, Inbar Mosseri, and Michal Irani. Imagic: Text-based real image editing with diffusion models. In *Proceedings of the IEEE Conference on Computer Vision and Pattern Recognition (CVPR)*, 2023. 2, 3

- [27] Junjie Ke, Qifei Wang, Yilin Wang, Peyman Milanfar, and Feng Yang. MUSIQ: Multi-scale image quality transformer. In *Proceedings of the IEEE International Conference on Computer Vision (ICCV)*. 6, 1
- [28] Boyi Li, Wenqi Ren, Dengpan Fu, Dacheng Tao, Dan Feng, Wenjun Zeng, and Zhangyang Wang. Benchmarking single-image dehazing and beyond. *IEEE Transactions on Image Processing (TIP)*, 2018. 4, 6
- [29] Boyun Li, Xiao Liu, Peng Hu, Zhongqin Wu, Jiancheng Lv, and Xi Peng. All-In-One image restoration for unknown corruption. In *Proceedings of the IEEE Conference on Computer Vision and Pattern Recognition (CVPR)*, 2022. 2
- [30] Boyun Li, Xiao Liu, Peng Hu, Zhongqin Wu, Jiancheng Lv, and Xi Peng. All-in-One image restoration for unknown corruption. In *Proceedings of the IEEE Conference on Computer Vision and Pattern Recognition (CVPR)*, 2022. 2
- [31] Ruoteng Li, Robby T Tan, and Loong-Fah Cheong. All-in-One bad weather removal using architectural search. In *Proceedings of the IEEE Conference on Computer Vision and Pattern Recognition (CVPR)*, 2020. 2
- [32] Bee Lim, Sanghyun Son, Heewon Kim, Seungjun Nah, and Kyoung Mu Lee. Enhanced deep residual networks for single image super-resolution. In *Proceedings of the IEEE Conference on Computer Vision and Pattern Recognition (CVPR) Workshops*, 2017. 6
- [33] Kechun Liu, Yitong Jiang, Inchang Choi, and Jinwei Gu. Learning image-adaptive codebooks for class-agnostic image restoration. *Proceedings of the IEEE International Conference on Computer Vision (ICCV)*, 2023. 2
- [34] Xingchao Liu, Xiwen Zhang, Jianzhu Ma, Jian Peng, and Qiang Liu. InstafLOW: One step is enough for high-quality diffusion-based text-to-image generation. *arXiv preprint arXiv:2309.06380*, 2023. 8
- [35] D. Martin, C. Fowlkes, D. Tal, and J. Malik. A database of human segmented natural images and its application to evaluating segmentation algorithms and measuring ecological statistics. In *Proceedings of the IEEE International Conference on Computer Vision (ICCV)*, 2001. 6
- [36] Sachit Menon, Alexandru Damian, Shijia Hu, Nikhil Ravi, and Cynthia Rudin. PULSE: Self-supervised photo upsampling via latent space exploration of generative models. In *Proceedings of the IEEE Conference on Computer Vision and Pattern Recognition (CVPR)*, 2020. 2
- [37] Yao Mingde, Huang Jie, Jin Xin, Xu Ruikang, Zhou Shenglong, Zhou Man, , and Xiong Zhiwei. Generalized lightness adaptation with channel selective normalization. In *Proceedings of the IEEE International Conference on Computer Vision (ICCV)*, 2023. 2
- [38] Seungjun Nah, Tae Hyun Kim, and Kyoung Mu Lee. Deep multi-scale convolutional neural network for dynamic scene deblurring. In *Proceedings of the IEEE Conference on Computer Vision and Pattern Recognition (CVPR)*, 2017. 6
- [39] Alex Nichol, Prafulla Dhariwal, Aditya Ramesh, Pranav Shyam, Pamela Mishkin, Bob McGrew, Ilya Sutskever, and Mark Chen. GLIDE: Towards photorealistic image generation and editing with text-guided diffusion models. 2021. 2
- [40] Xingang Pan, Xiaohang Zhan, Bo Dai, Dahua Lin, Chen Change Loy, and Ping Luo. Exploiting deep generative prior for versatile image restoration and manipulation. *IEEE Transactions on Pattern Analysis and Machine Intelligence (TPAMI)*, 44(11):7474–7489, 2021. 2
- [41] Dongwon Park, Byung Hyun Lee, and Se Young Chun. All-in-One image restoration for unknown degradations using adaptive discriminative filters for specific degradations. In *Proceedings of the IEEE Conference on Computer Vision and Pattern Recognition (CVPR)*, 2023. 2
- [42] Rui Qian, Robby T Tan, Wenhan Yang, Jiajun Su, and Jiaying Liu. Attentive generative adversarial network for rain-drop removal from a single image. In *Proceedings of the IEEE Conference on Computer Vision and Pattern Recognition (CVPR)*, 2018. 6
- [43] Rui Qian, Robby T Tan, Wenhan Yang, Jiajun Su, and Jiaying Liu. Attentive generative adversarial network for rain-drop removal from a single image. In *Proceedings of the IEEE Conference on Computer Vision and Pattern Recognition (CVPR)*, 2018. 2
- [44] Xu Qin, Zhilin Wang, Yuanchao Bai, Xiaodong Xie, and Huizhu Jia. FFA-Net: Feature fusion attention network for single image dehazing. In *Proceedings of the AAAI Conference on Artificial Intelligence*, 2020. 2
- [45] Yuhui Quan, Mingqin Chen, Tongyao Pang, and Hui Ji. Self2Self with dropout: Learning self-supervised denoising from single image. In *Proceedings of the IEEE Conference on Computer Vision and Pattern Recognition (CVPR)*, 2020. 2
- [46] Alec Radford, Jong Wook Kim, Chris Hallacy, Aditya Ramesh, Gabriel Goh, Sandhini Agarwal, Girish Sastry, Amanda Askell, Pamela Mishkin, Jack Clark, et al. Learning transferable visual models from natural language supervision. In *Proceedings of International Conference on Machine Learning (ICML)*, 2021. 2, 3
- [47] Aditya Ramesh, Prafulla Dhariwal, Alex Nichol, Casey Chu, and Mark Chen. Hierarchical text-conditional image generation with clip latents. *arXiv preprint arXiv:2204.06125*, 2022. 2
- [48] Dongwei Ren, Wangmeng Zuo, Qinghua Hu, Pengfei Zhu, and Deyu Meng. Progressive image deraining networks: A better and simpler baseline. In *Proceedings of the IEEE Conference on Computer Vision and Pattern Recognition (CVPR)*, 2019. 2
- [49] Robin Rombach, Andreas Blattmann, Dominik Lorenz, Patrick Esser, and Björn Ommer. High-resolution image synthesis with latent diffusion models. In *Proceedings of the IEEE Conference on Computer Vision and Pattern Recognition (CVPR)*, 2022. 2, 3, 5, 6, 7, 8
- [50] Olaf Ronneberger, Philipp Fischer, and Thomas Brox. U-Net: Convolutional networks for biomedical image segmentation. In *Proceedings of Medical Image Computing and Computer-Assisted Intervention (MICCAI)*, 2015. 5
- [51] Chitwan Saharia, William Chan, Saurabh Saxena, Lala Li, Jay Whang, Emily L Denton, Kamyar Ghasemipour, Raphael Gontijo Lopes, Burcu Karagol Ayan, Tim Salimans, et al. Photorealistic text-to-image diffusion models with deep



- language understanding. *Proceedings of Advances in Neural Information Processing Systems (NeurIPS)*, 2022. 2
- [52] Hamid R Sheikh, Muhammad F Sabir, and Alan C Bovik. A statistical evaluation of recent full reference image quality assessment algorithms. *IEEE Transactions on Image Processing (TIP)*, 2006. 3
- [53] Ziyi Shen, Wenguan Wang, Jianbing Shen, Haibin Ling, Tingfa Xu, and Ling Shao. Human-aware motion deblurring. In *Proceedings of the IEEE International Conference on Computer Vision (ICCV)*, 2019. 6
- [54] Amanpreet Singh, Ronghang Hu, Vedanuj Goswami, Guillaume Couairon, Wojciech Galuba, Marcus Rohrbach, and Douwe Kiela. Flava: A foundational language and vision alignment model. In *Proceedings of the IEEE Conference on Computer Vision and Pattern Recognition (CVPR)*, 2022. 6
- [55] Yuda Song, Zhuqing He, Hui Qian, and Xin Du. Vision transformers for single image dehazing. *IEEE Transactions on Image Processing (TIP)*, 2023. 2
- [56] Ming Tao, Hao Tang, Fei Wu, Xiao-Yuan Jing, Bing-Kun Bao, and Changsheng Xu. DF-GAN: A simple and effective baseline for text-to-image synthesis. In *Proceedings of the IEEE Conference on Computer Vision and Pattern Recognition (CVPR)*, 2022. 2
- [57] Ming-Feng Tsai, Tie-Yan Liu, Tao Qin, Hsin-Hsi Chen, and Wei-Ying Ma. FRank: a ranking method with fidelity loss. In *ACM SIGGRAPH Conference Proceedings*, 2007. 3
- [58] Jeya Maria Jose Valanarasu, Rajeev Yasarla, and Vishal M Patel. Transweather: Transformer-based restoration of images degraded by adverse weather conditions. In *Proceedings of the IEEE Conference on Computer Vision and Pattern Recognition (CVPR)*, 2022. 2
- [59] Aaron Van Den Oord, Oriol Vinyals, et al. Neural discrete representation learning. *Proceedings of Advances in Neural Information Processing Systems (NeurIPS)*, 2017. 2
- [60] Ashish Vaswani, Noam Shazeer, Niki Parmar, Jakob Uszkoreit, Llion Jones, Aidan N Gomez, Łukasz Kaiser, and Illia Polosukhin. Attention is all you need. 2017. 5
- [61] Jianyi Wang, Kelvin CK Chan, and Chen Change Loy. Exploring CLIP for assessing the look and feel of images. In *Proceedings of the AAAI Conference on Artificial Intelligence*, 2023. 6
- [62] Jianyi Wang, Zongsheng Yue, Shangchen Zhou, Kelvin CK Chan, and Chen Change Loy. Exploiting diffusion prior for real-world image super-resolution. In *arXiv preprint arXiv:2305.07015*, 2023. 2, 6
- [63] Jianyi Wang, Zongsheng Yue, Shangchen Zhou, Kelvin CK Chan, and Chen Change Loy. Exploiting diffusion prior for real-world image super-resolution. In *arXiv preprint arXiv:2305.07015*, 2023. 8
- [64] Peng Wang, An Yang, Rui Men, Junyang Lin, Shuai Bai, Zhikang Li, Jianxin Ma, Chang Zhou, Jingren Zhou, and Hongxia Yang. Ofa: Unifying architectures, tasks, and modalities through a simple sequence-to-sequence learning framework. In *Proceedings of International Conference on Machine Learning (ICML)*, 2022. 6
- [65] Xintao Wang, Liangbin Xie, Chao Dong, and Ying Shan. Real-ESRGAN: Training real-world blind super-resolution with pure synthetic data. In *Proceedings of the IEEE International Conference on Computer Vision (ICCV)*, 2021. 6
- [66] Yinhuai Wang, Jiwen Yu, and Jian Zhang. Zero-shot image restoration using denoising diffusion null-space model. In *Proceedings of International Conference on Learning Representations (ICLR)*, 2023. 2
- [67] Chen Wei, Wenjing Wang, Wenhan Yang, and Jiaying Liu. Deep retinex decomposition for low-light enhancement. *Proceedings of The British Machine Vision Conference (BMVC)*, 2018. 6
- [68] Jay Whang, Mauricio Delbracio, Hossein Talebi, Chitwan Saharia, Alexandros G Dimakis, and Peyman Milanfar. Deblurring via stochastic refinement. In *Proceedings of the IEEE Conference on Computer Vision and Pattern Recognition (CVPR)*, 2022. 2
- [69] Tao Xu, Pengchuan Zhang, Qiuyuan Huang, Han Zhang, Zhe Gan, Xiaolei Huang, and Xiaodong He. AttnGAN: Fine-grained text to image generation with attentional generative adversarial networks. In *Proceedings of the IEEE Conference on Computer Vision and Pattern Recognition (CVPR)*, 2018. 2
- [70] Tao Yang, Peiran Ren, Xuansong Xie, and Lei Zhang. GAN prior embedded network for blind face restoration in the wild. In *Proceedings of the IEEE Conference on Computer Vision and Pattern Recognition (CVPR)*, 2021. 2
- [71] Wenhan Yang, Robby T Tan, Jiashi Feng, Jiaying Liu, Zongming Guo, and Shuicheng Yan. Deep joint rain detection and removal from a single image. In *Proceedings of the IEEE Conference on Computer Vision and Pattern Recognition (CVPR)*, 2017. 6
- [72] Hui Ye, Xiulong Yang, Martin Takac, Rajshekhar Sunderraman, and Shihao Ji. Improving text-to-image synthesis using contrastive learning. *Proceedings of The British Machine Vision Conference (BMVC)*, 2021. 2
- [73] Han Zhang, Jing Yu Koh, Jason Baldridge, Honglak Lee, and Yinfei Yang. Cross-modal contrastive learning for text-to-image generation. In *Proceedings of the IEEE Conference on Computer Vision and Pattern Recognition (CVPR)*, 2021. 2
- [74] Jinghao Zhang, Jie Huang, Mingde Yao, Zizheng Yang, Hu Yu, Man Zhou, and Feng Zhao. Ingredient-oriented multi-degradation learning for image restoration. In *Proceedings of the IEEE Conference on Computer Vision and Pattern Recognition (CVPR)*, 2023. 2
- [75] Richard Zhang, Phillip Isola, Alexei A Efros, Eli Shechtman, and Oliver Wang. The unreasonable effectiveness of deep features as a perceptual metric. In *Proceedings of the IEEE Conference on Computer Vision and Pattern Recognition (CVPR)*, 2018. 6, 8
- [76] Zhaoyang Zhang, Yitong Jiang, Jun Jiang, Xiaogang Wang, Ping Luo, and Jinwei Gu. STAR: A structure-aware lightweight transformer for real-time image enhancement. In *Proceedings of the IEEE International Conference on Computer Vision (ICCV)*, 2021. 2
- [77] Zhixing Zhang, Ligong Han, Arnab Ghosh, Dimitris N Metaxas, and Jian Ren. SINE: Single image editing with text-to-image diffusion models. In *Proceedings of the IEEE*

- Conference on Computer Vision and Pattern Recognition (CVPR)*, 2023. 2, 3
- [78] Zhaoyang Zhang, Yitong Jiang, Wenqi Shao, Xiaogang Wang, Ping Luo, Kaimo Lin, and Jinwei Gu. Real-time controllable denoising for image and video. In *Proceedings of the IEEE Conference on Computer Vision and Pattern Recognition (CVPR)*, 2023. 2
- [79] Shangchen Zhou, Kelvin Chan, Chongyi Li, and Chen Change Loy. Towards robust blind face restoration with codebook lookup transformer. *Proceedings of Advances in Neural Information Processing Systems (NeurIPS)*, 2022. 2
- [80] Yuqian Zhou, David Ren, Neil Emerton, Sehoon Lim, and Timothy Large. Image restoration for under-display camera. *Proceedings of the IEEE Conference on Computer Vision and Pattern Recognition (CVPR)*, 2021. 6, 3
- [81] Yuqian Zhou, David Ren, Neil Emerton, Sehoon Lim, and Timothy Large. Image restoration for under-display camera. In *Proceedings of the IEEE Conference on Computer Vision and Pattern Recognition (CVPR)*, 2021. 4, 6, 8
- [82] Minfeng Zhu, Pingbo Pan, Wei Chen, and Yi Yang. DM-GAN: Dynamic memory generative adversarial networks for text-to-image synthesis. In *Proceedings of the IEEE Conference on Computer Vision and Pattern Recognition (CVPR)*, 2019. 2
- [83] Xizhou Zhu, Jinguo Zhu, Hao Li, Xiaoshi Wu, Hongsheng Li, Xiaohua Wang, and Jifeng Dai. Uni-perceiver: Pre-training unified architecture for generic perception for zero-shot and few-shot tasks. In *Proceedings of the IEEE Conference on Computer Vision and Pattern Recognition (CVPR)*, 2022. 6

# AutoDIR: Automatic All-in-One Image Restoration with Latent Diffusion

## Supplementary Material

This supplementary is organized as followed:

- In Sec. 6, we first introduce our user interaction application, highlighting its significance in enhancing user engagement.
- Next, in Sec. 7, we present the detailed training and testing settings employed in our study.
- To further validate the effectiveness of our proposed approach, we present additional qualitative and quantitative results in Sec. 8.1, including seven image restoration tasks: denoising, super-resolution, deblurring, deraining, dehazing, low light enhancement, and deraindrop removal.
- In Sec. 8.2, we conduct additional ablation studies focusing on the semantic-agnostic constraint and the structural-correction module, providing deeper insights into their contributions.
- To address the reconstruction of images affected by multiple unknown degradations, we present further results in an iterative process in Sec. 8.3.
- In order to evaluate the generalizability of AutoDIR, we conduct experiments in Sec. 8.4, where we investigate its ability to be fast finetuned for new image restoration tasks.
- In Sec. 8.5, we conduct a user study specifically targeting the denoising task. This study aims to provide additional evidence regarding the perceptual quality and effectiveness of AutoDIR in comparison to alternative methods.
- In the attached video, we also provide a captivating demonstration of AutoDIR’s working mechanism, accompanied by visual results that highlight its superior performance compared to baseline methods.

## 6. User Interaction

AutoDIR also provides a customizable approach to tailor the result outputs based on user preferences. Users can effectively modify the input image by providing corresponding text prompts. Furthermore, we also utilize classifier-free [19] to enable the adjustment of weights for fine-tuning the desired enhancements. As depicted in Fig. 11, the Blind Image Quality Assessment (BIQA) model automatically suggests denoising options, and the user further brightens the image according to his preference by providing the corresponding text prompt. Additionally, the editing strength can be enhanced by adjusting the weight to increase the brightness of the image. The support of user interaction highlights the flexibility and adaptability of our proposed approach, allowing for a highly customizable image enhancement experience.

## 7. Implementation Details

Our experiments are conducted using PyTorch on a computational setup comprising eight NVIDIA V100 GPUs. The training process for the AutoDIR framework involves three distinct steps. Firstly, we initialize the training by freezing the text encoder and fine-tuning the image encoder within the Blind Image Quality Assessment (BIQA) module. We utilize the Adam optimizer with a batch size of 1024 and train for 200 epochs. The initial learning rate is set to  $3 \times 10^{-6}$  and follows a cosine annealing rule. Next, we proceed to fine-tune the All-in-One Image Restoration Module (AIR) using the Adam optimizer. During this stage, we employ a learning rate of  $1e^{-4}$  and a batch size of 256. The fine-tuning process is performed for 180 epochs. Finally, we freeze the previously trained pipeline components and focus on training the structural-correction module (SCM). For this stage, we employ the Adam optimizer and a cosine annealing rule. The initial learning rate is set to  $1e^{-3}$ , and the batch size is 256. We train the SCM for 4,000 iterations. In our experiments, the structural-correction module is based on NAFNet architecture [10]. During inference, the coefficient  $w$  of the structural-correction module is set to be 1 as default for denoising, deraining, dehazing, deraindrop, low light enhancement, and deblurring tasks and 0.1 for the super-resolution task to maintain the generation capability of the All-in-one Image Restoration (AIR) module.

## 8. Extensive Experimental Results

This section provides additional visualizations and experimental details on additional datasets and training settings in Sec. 4 of the main text.

### 8.1. Results on Seven Joint-learned Tasks

**Deblurring.** On the challenging task of deblurring, our method attains superior results compared to its counterparts, as evident in Tab. 4. For instance, our method surpasses the next-best result by a significant margin of 8.9 in terms of the MUSIQ score [27]. Additionally, the accompanying Fig. 18 demonstrates the capabilities of our approach in handling complex scenes affected by substantial blur. In contrast, alternative methods either struggle to effectively execute deblurring or exhibit inadequate reduction of blurriness.

**Super Resolution.** As illustrated in Tab. 5, our method demonstrates competitive performance across various metrics at both  $\times 8$  and  $\times 4$  scales, surpassing other baselines by a remarkable lead of 12.48 points in MUSIQ score [27].



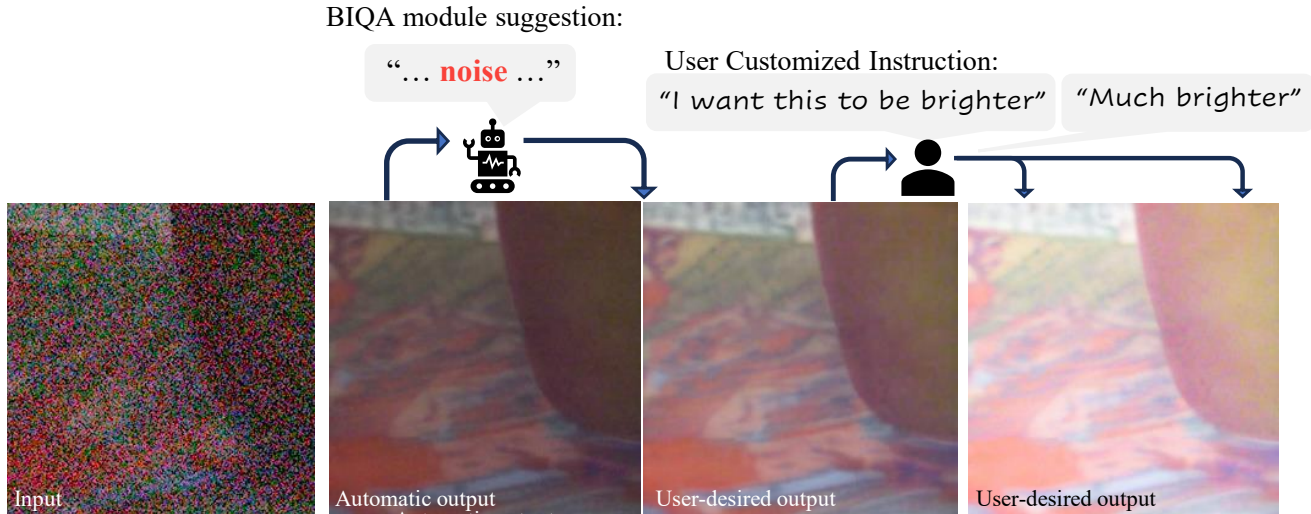


Figure 11. User specified results.

Table 4. Quantitative comparison on deblurring task. PSNR/MUSIQ/CLIP-IQA  $\uparrow$ : the higher, the better; DISTS/LPIPS $\downarrow$ : the lower, the better.

Method	GoPro					HIDE				
	DISTS	MUSIQ	CLIP-IQA	PSNR	LPIPS	DISTS	MUSIQ	CLIP-IQA	PSNR	LPIPS
NAFNet	<u>0.149</u>	43.28	0.221	<u>26.67</u>	<u>0.208</u>	0.379	38.02	0.165	<u>24.66</u>	<u>0.262</u>
SD	0.157	<u>44.83</u>	<u>0.255</u>	22.53	0.241	<u>0.203</u>	<u>40.08</u>	<u>0.205</u>	22.72	0.276
<b>Ours</b>	<b>0.117</b>	<b>53.73</b>	<b>0.278</b>	<b>26.86</b>	<b>0.156</b>	<b>0.139</b>	<b>52.68</b>	<b>0.212</b>	<b>25.26</b>	<b>0.181</b>

Fig. 19 and 20 highlight the capabilities of our method in generating more authentic and detailed content, such as animal fur and complex building structures, demonstrating the effectiveness of our approach in enhancing image resolution.

**Denoising.** Fig. 21 and 22 visually illustrate our method’s ability to restore fine details while preserving the underlying object structures, reaffirming the effectiveness of the AutoDIR framework.

**Deraindrop.** As illustrated in the accompanying Fig. 23, our method effectively eliminates raindrops and successfully restores background details, resulting in a visually pleasing output. It is worth noting that NAFNet [10] is incapable of addressing this specific task of raindrop removal, while SD (Stable Diffusion) [49] falls short of completely eliminating the raindrop effect.

**Deraining.** the representations in Fig. 24 provide strong evidence of the superior performance of our pipeline compared to competing baselines in terms of qualitative outcomes.

**Dehazing.** Fig. 25 emphasizes AutoDIR’s smoother and more consistent visual quality compared to alternative approaches.

**Low Light Enhancement.** Fig. 26 illustrates the effectiveness of our method in reducing noise compared to NAFNet [10], as well as minimizing distortion when compared to Stable Diffusion (SD)[49].

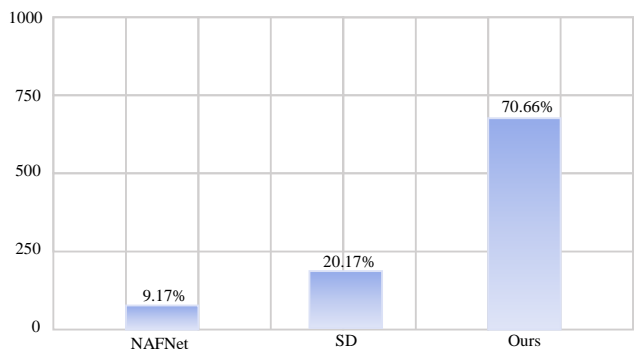


Figure 12. Results of the user study on 18 denoising images. We collected 51 forms and  $18 \times 51 = 918$  responses in total. Among them, AutoDIR receives more than 70% of the votes.

Table 5. Quantitative comparison on single image super-resolution  $\times 4$  and  $\times 8$  tasks. PSNR/MUSIQ/CLIP-IQA  $\uparrow$ : the higher, the better; DISTSLPIPS: the lower, the better.

Method	DIV2K $\times 4$					DIV2K $\times 8$				
	DISTS	MUSIQ	CLIP-IQA	PSNR	LPIPS	DISTS	MUSIQ	CLIP-IQA	PSNR	LPIPS
NAFNet	<u>0.214</u>	39.01	0.347	<b>28.49</b>	0.415	0.313	21.31	0.279	<b>24.52</b>	0.554
SD	0.262	<u>39.58</u>	<u>0.366</u>	27.04	<u>0.307</u>	<u>0.238</u>	<u>33.54</u>	<u>0.365</u>	23.48	<u>0.380</u>
Ours	<b>0.156</b>	<b>52.01</b>	<b>0.501</b>	<u>27.32</u>	<b>0.225</b>	<b>0.215</b>	<b>48.99</b>	<b>0.472</b>	<u>23.57</u>	<b>0.301</b>

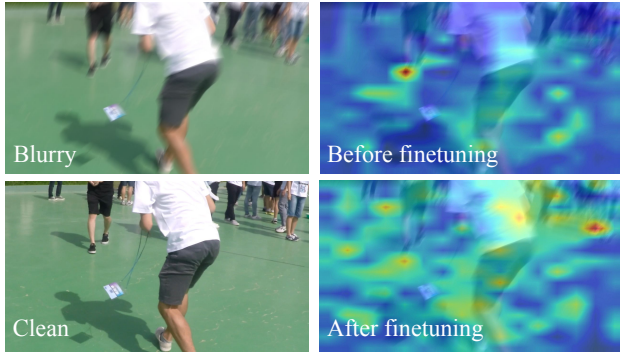


Figure 13. Self-attention maps of BIQA image encoder. Attention maps focus on (have the highest attention values) the foreground object in BIQA image encoder without fine-tuning, while attention maps focus on (have the highest attention values) both foreground and background objects in BIQA image encoder fine-tuned with SA constraint.

## 8.2. Ablation Studies

### Fine-tuning with Semantic-agnostic Constraint for BIQA Model

In order to further analyze the effectiveness of our semantic-agnostic constraint, we visualize the attention map of the image encoder in Fig. 13. As depicted in the visualization, prior to fine-tuning, the attention map primarily focuses on the pronominal object, which is consistent with the behavior of the original CLIP model [46] that was pre-trained on image classification tasks. After fine-tuning with semantic-agnostic constraint, we observe that the attention maps expand to highlight background areas that may contain potential artifacts which shows that the BIQA model has successfully learned to prioritize and focus on artifacts, leading to more accurate BIQA results.

### Importance of Structural-Correction Module (SCM)

The generative Stable Diffusion model [49] has demonstrated a strong ability to generate unseen features. However, it falls short when it comes to preserving the original structural information of the input image, which is crucial for image enhancement tasks.

To address this limitation, we have designed the structural-correction module. This module aims to preserve the original texture of input images, especially in cases

where generative-based models tend to distort fine details such as human faces and text.

As illustrated in Fig. 14, AutoDIR with the SCM produces high-quality results with fine details intact. On the other hand, the model without the SCM exhibits significant distortion in faces and text. Moreover, Fig. 15 demonstrates that SCM also shows the ability to correct hallucinated undesired textures of the results of the AIR module.

## 8.3. Results on Multiple Unknown Degradations

We present additional visualization results in Fig. 16 on images with multiple unknown degradations on UCD [80] and EVUP [22] datasets, to further demonstrate the performance of our method in handling such complex scenarios.

## 8.4. Generalizability of All-in-one Image Restoration Module

In addition to the experiments conducted on fine-tuning for the de-snowing image restoration task in Section 4.3, we further investigate and conduct supplementary experiments on JPEG restoration task. We explore a more challenging setting using a limited dataset of 40 pairs of compressed-clean images from the LIVE dataset [52]. We initialize the AIR module with pre-trained weights and fine-tune it for 15 epochs. Figure 17 demonstrates that the model, with pre-trained AIR weights, exhibits improved efficiency in handling JPEG compression tasks.

## 8.5. User Study

To further examine the effectiveness of AutoDIR, we conduct a user study on the denoising task with 9 synthetic noisy images and 9 real noise images. We compare AutoDIR with NAFNet [10] and Stable Diffusion [49]. As shown in Fig. 27, given the input and ground-truth clean image, the question is to ask which the best denoising image is and the choices are in random orders. We collect 51 forms and there are  $51 \times 18 = 918$  responses in total. Fig. 12 illustrates that AutoDIR gathers more than 70% of the votes for producing the best denoising results.



Figure 14. Qualitative comparisons for AutoDIR with/without SCM module on dehazing and deraindrop tasks.

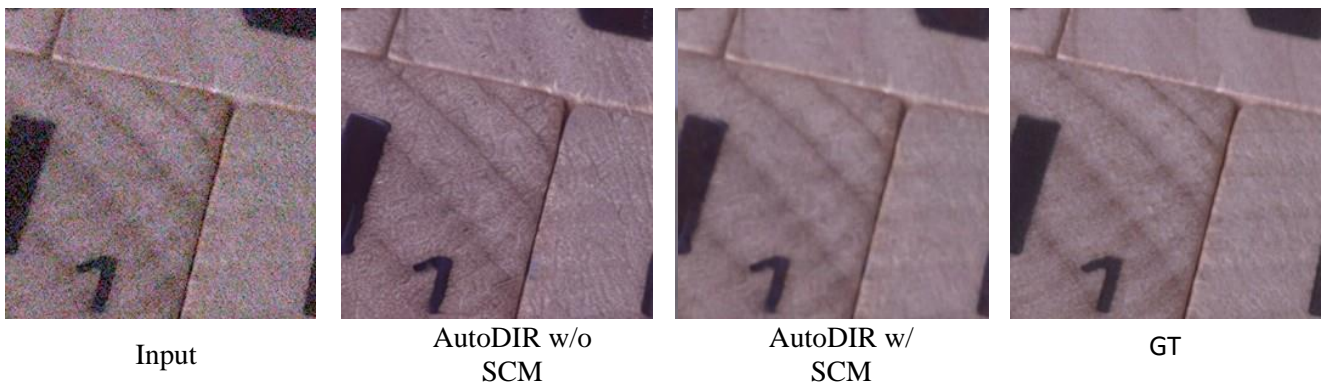


Figure 15. Qualitative comparisons for AutoDIR with/without SCM module on denoising tasks.



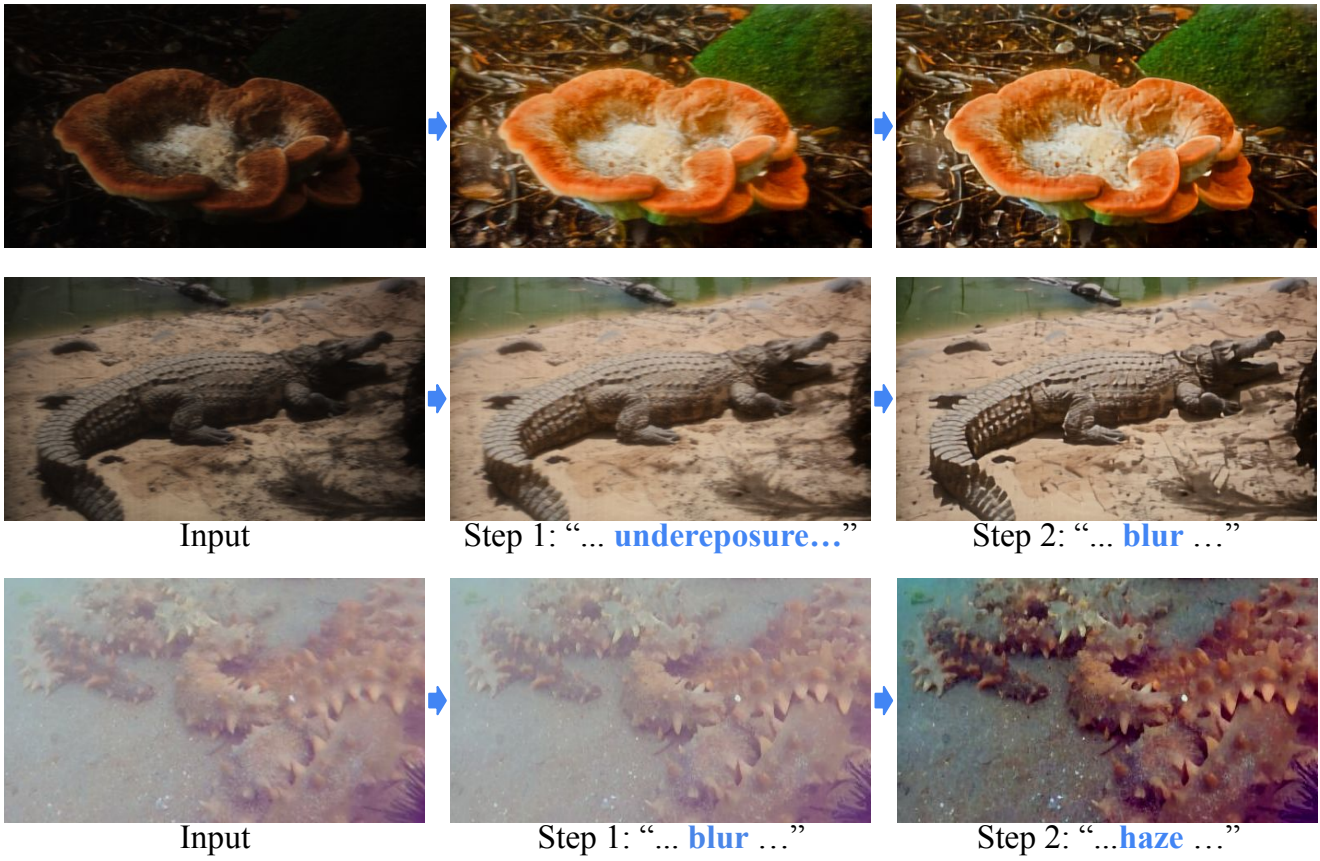


Figure 16. Qualitative illustration of how AutoDIR handles multiple artifacts iteratively.



Input



NAFNet



Initialize with SD weight



Initialize with AIR weight



GT



Figure 17. Qualitative comparisons on for transfer learning on JPEG task

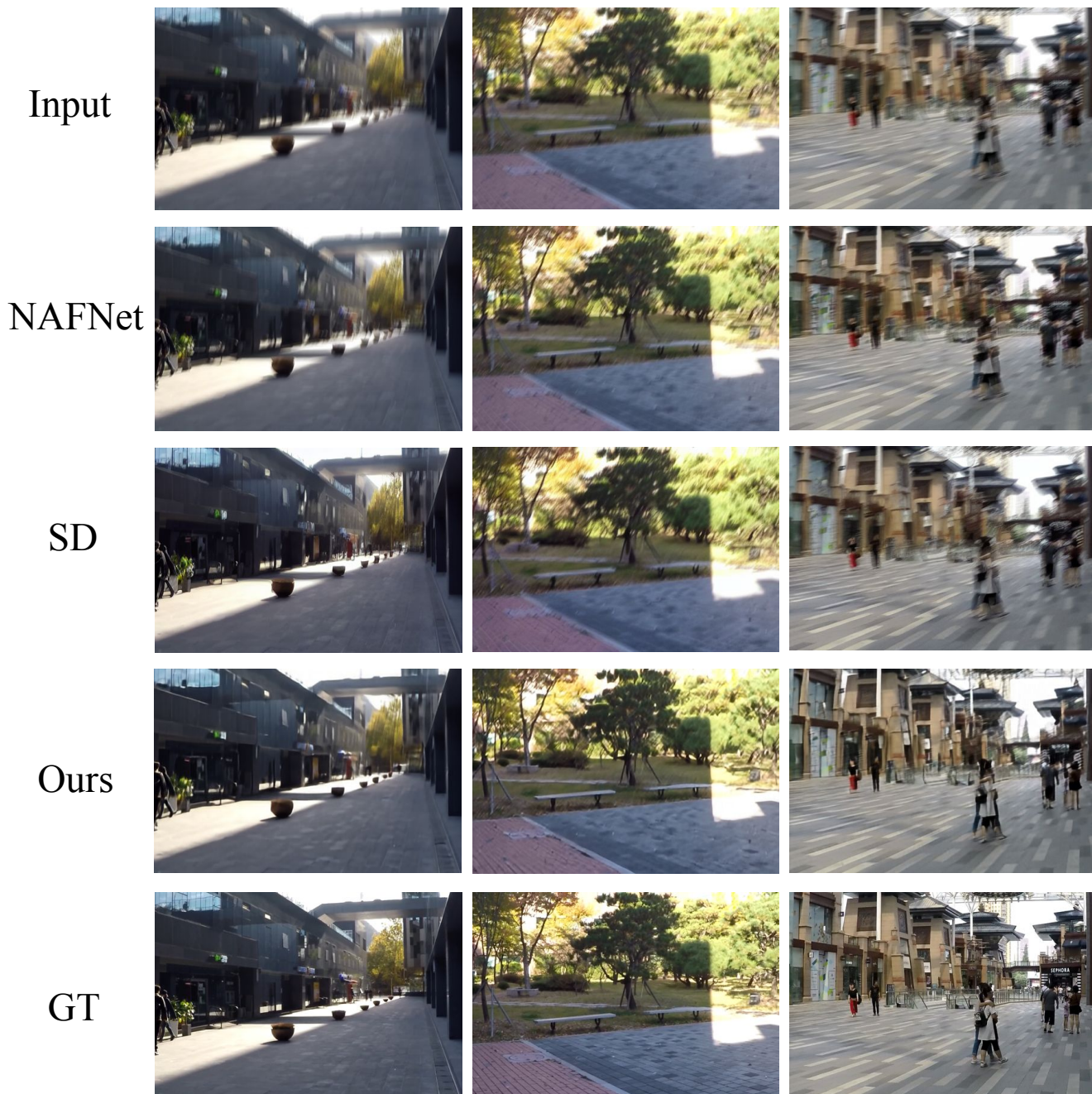


Figure 18. Qualitative comparisons on deblurring task

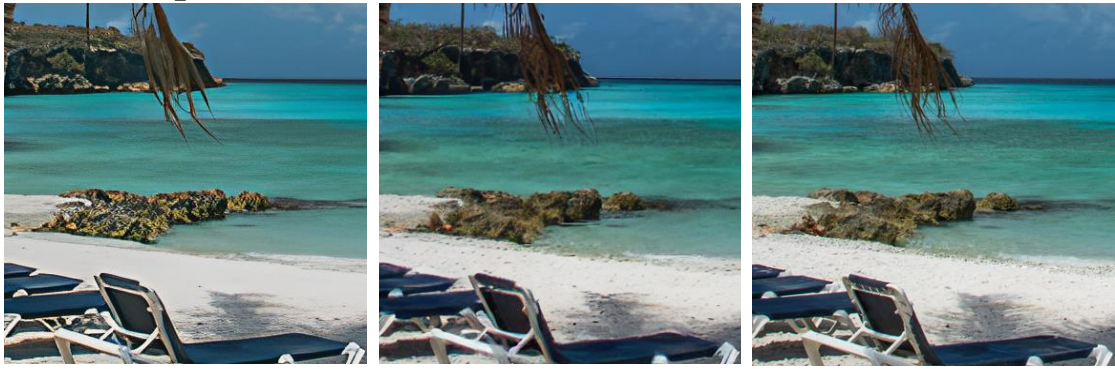




Input

NAFNet

SD



StableSR

Ours

GT



Input

NAFNet

SD



StableSR

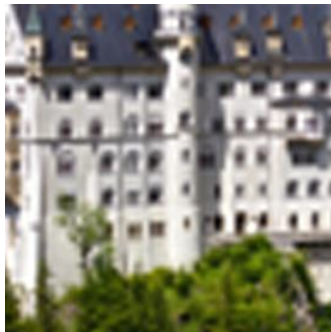
Ours

GT

Figure 19. Qualitative comparisons  $\times 4$  super-resolution



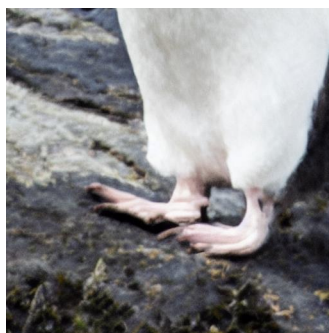
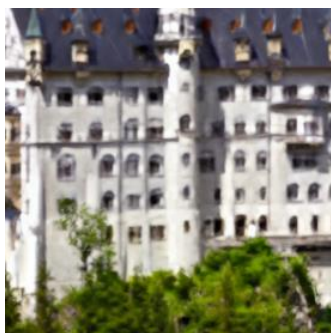
Input



NAFNet



SD



Ours



GT

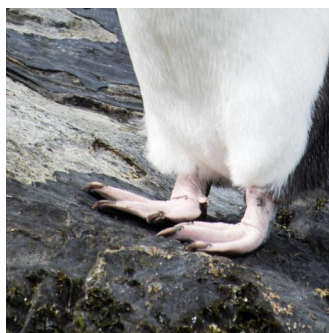


Figure 20. Qualitative comparisons  $\times 8$  super-resolution

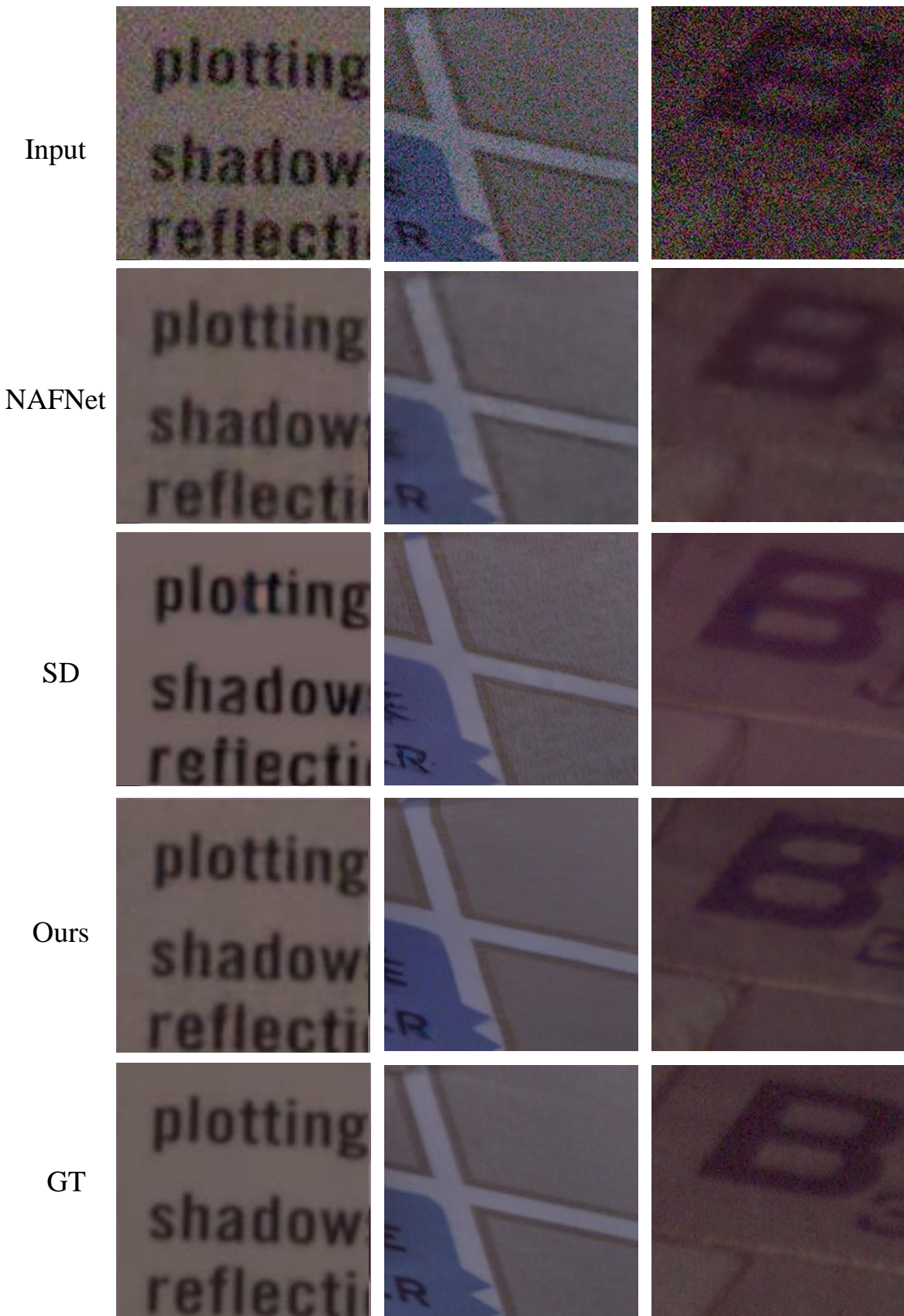


Figure 21. Qualitative comparisons on SIDD real noise task



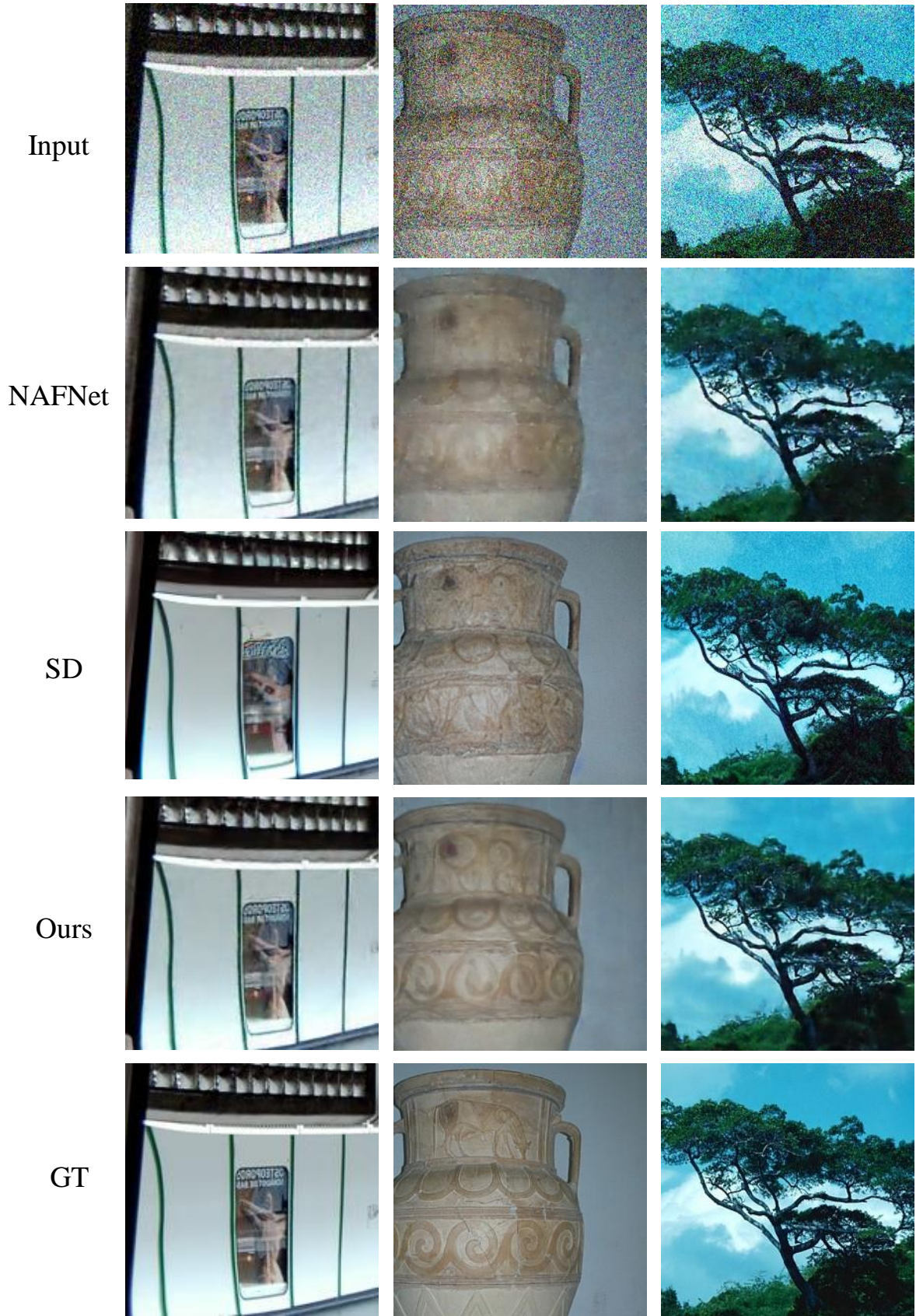


Figure 22. Qualitative comparisons on synthetic denoise task



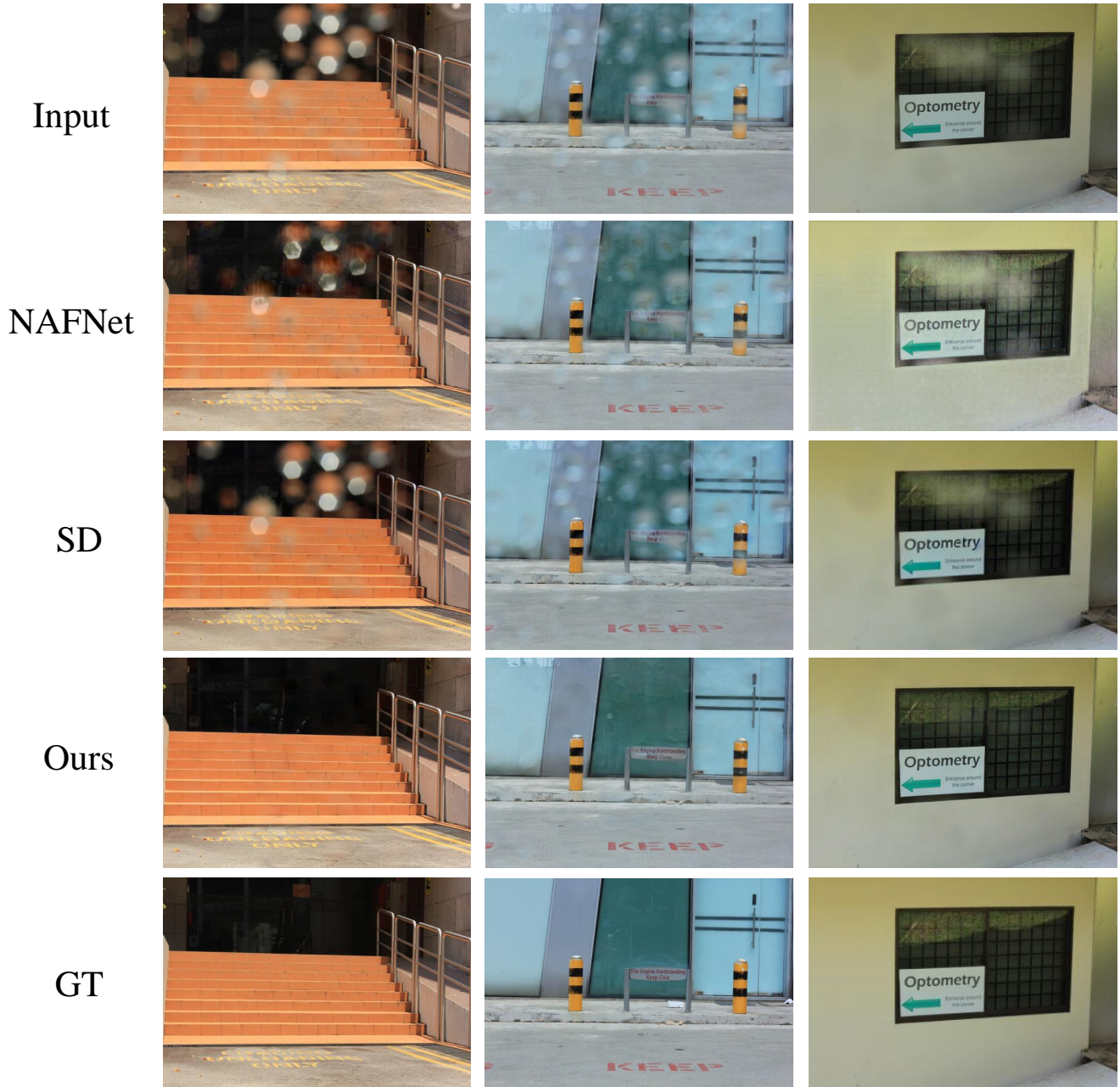


Figure 23. Qualitative comparisons on deraindrop task

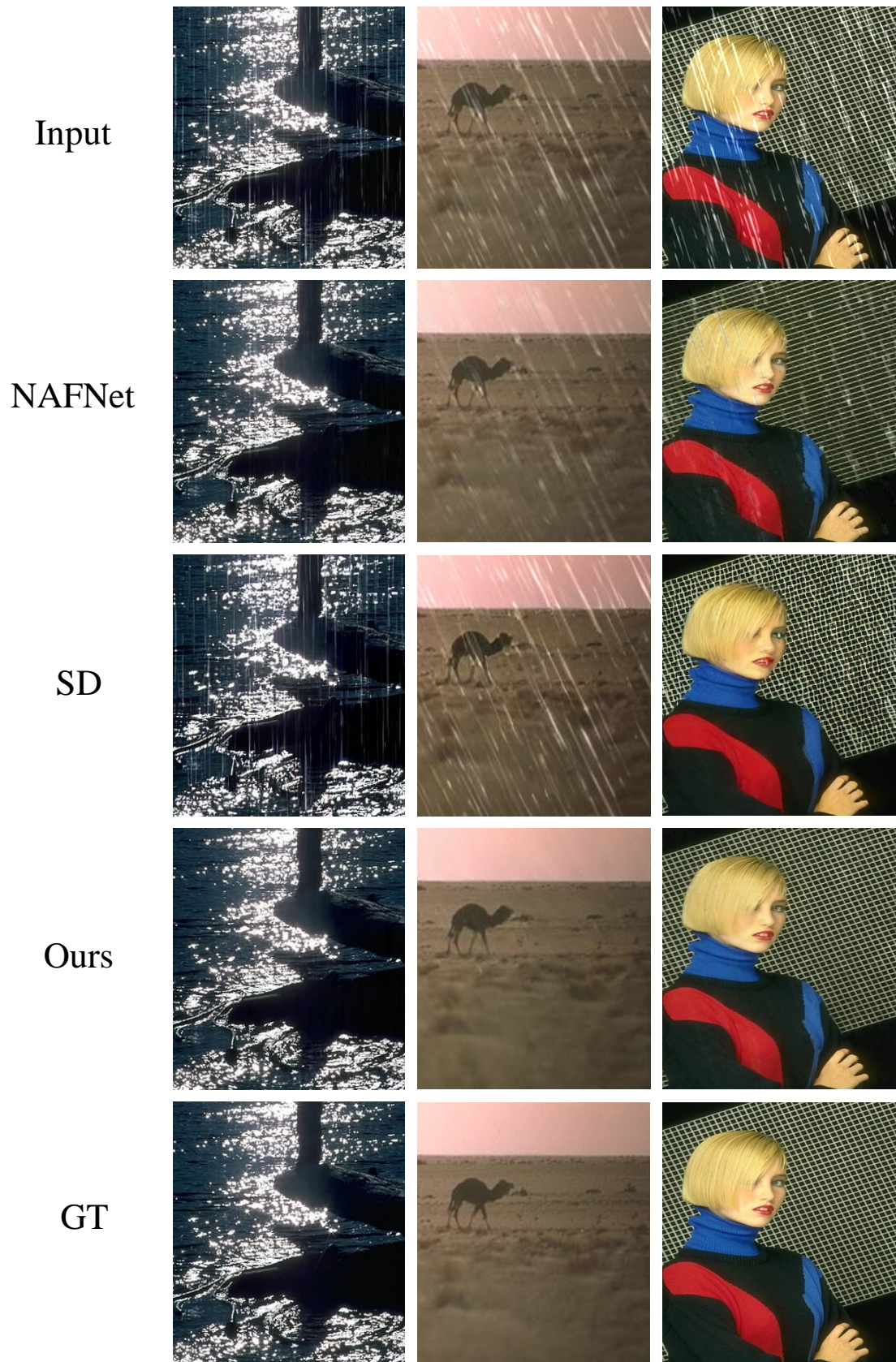


Figure 24. Qualitative comparisons on deraining task



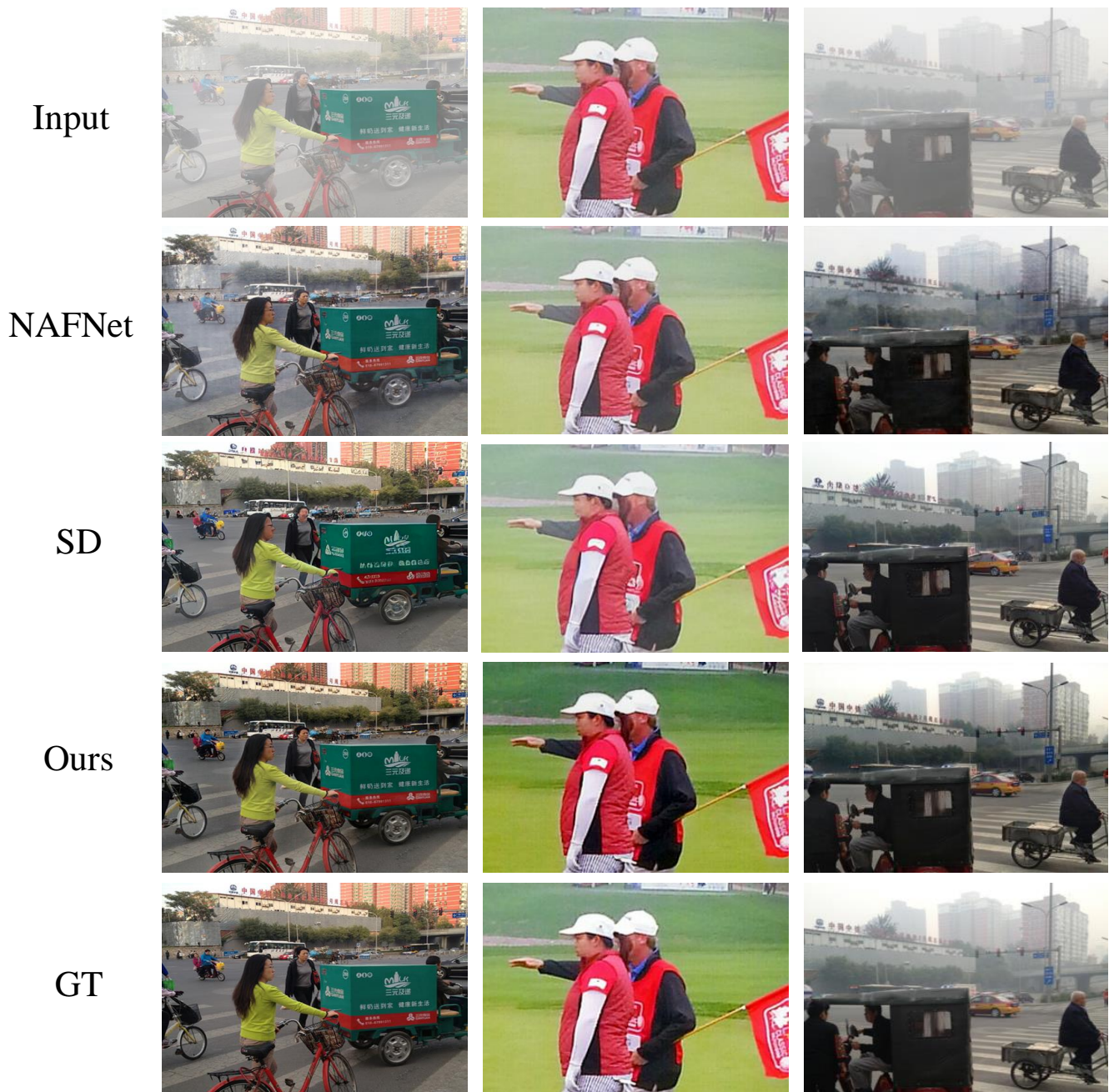


Figure 25. Qualitative comparisons on dehazing task



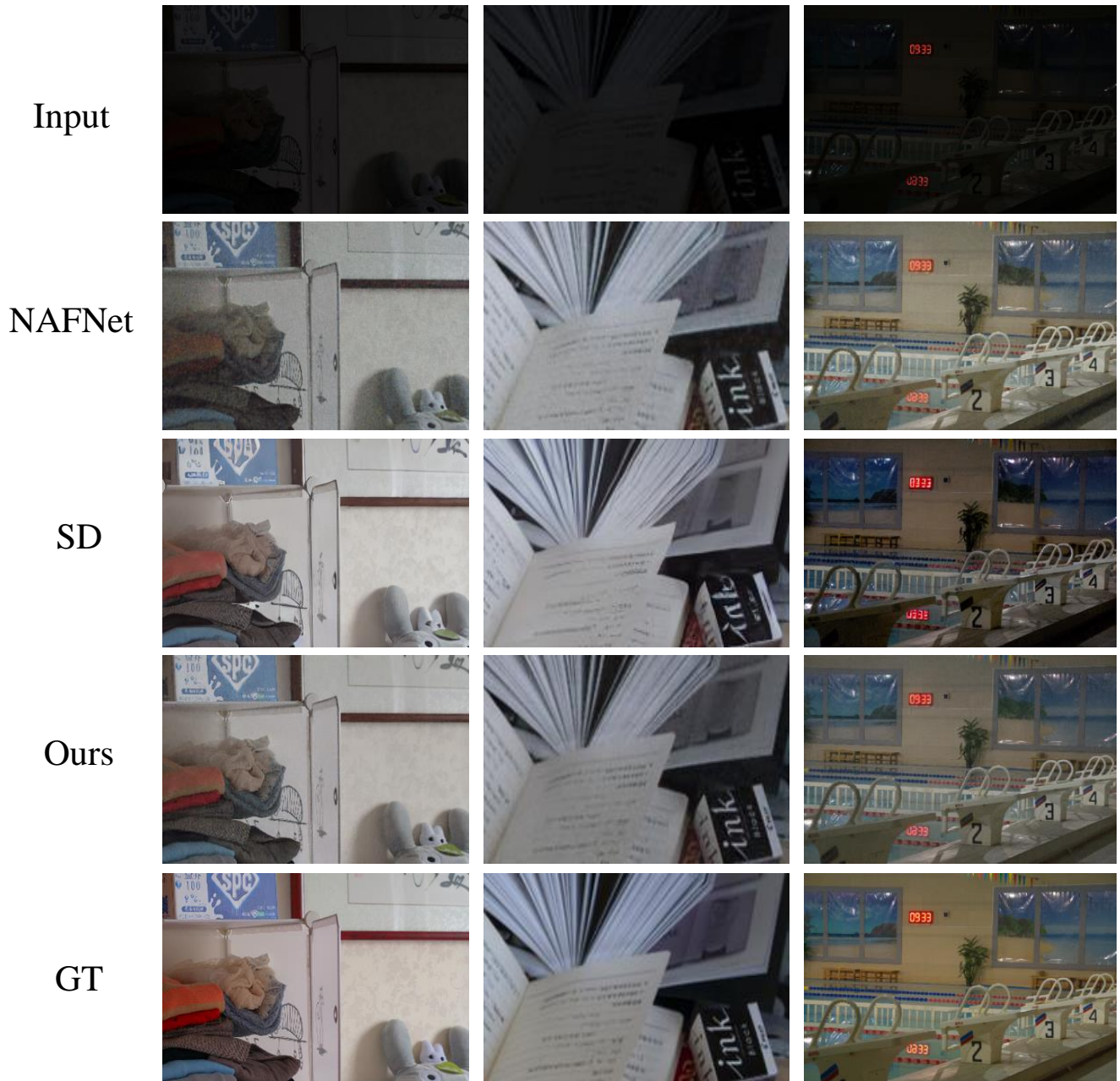
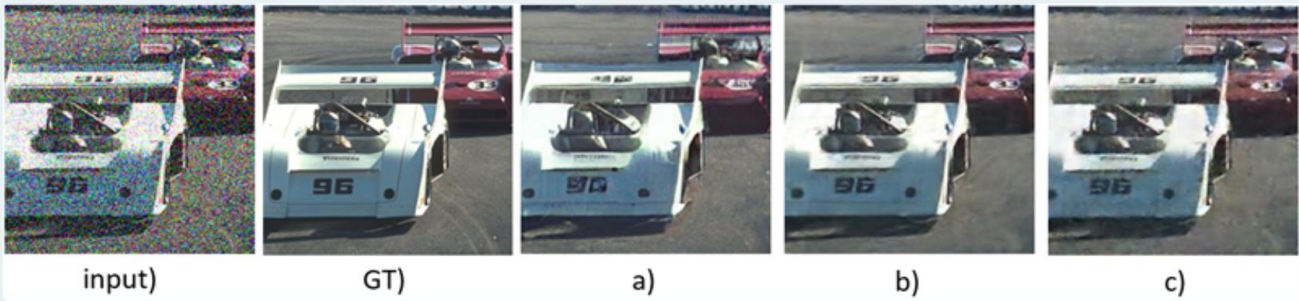


Figure 26. Qualitative comparisons on low light image enhancement task

5

Which of the following has the best denoising result?



- A
- B
- C

Figure 27. Screenshot of the user interface in the user study.